Electronic and structural disorder of NiCo2O4 nanostructures using phytochemicals from desert gourd offered efficient asymmetric supercapacitor and oxygen evolution reaction

Shusheel Kumar, Aneela Tahira, Adeel Liaquat Bhatti, Umair Aftab, Ayman Nafady, Sooraj Kumar, Mélanie Emo, Brigitte Vigolo, Antonia Infantes-Molin, Elmuez Dawi, et al.

Electronic and structural disorder of $NiCo_2O_4$ Nanostructures using phytochemicals from desert gourd offered efficient asymmetric supercapacitor and oxygen evolution reaction

Shusheel Kumar[a], Aneela Tahira[c], Adeel Liaquat Bhatti[a], Umair Aftab[e], Ayman Nafady[k], Sooraj Kumar[d], Mélanie Emo[f], Brigitte Vigolo[f], Antonia Infantes-Molin[g], Elmuez Dewai[j], Alberto Vomiero[h,i*], Zafar Hussain Ibupoto[*b]

[a]Institute of Physics, University of Sindh Jamshoro, 76080, Sindh Pakistan

[b]Institute of Chemistry, University of Sindh Jamshoro, 76080, Sindh Pakistan

[c]Institute of Chemistry, Shah Abdul Latif University Khairpur Mirs, Sindh, Pakistan

[d]Department of Chemical Engineering, Mehran University of Engineering and Technology, 7680 Jamshoro, Sindh Pakistan

[e]Department of Metallurgy and Materials, Mehran University of Engineering and Technology, 7680 Jamshoro, Sindh Pakistan

[f]Université de Lorraine, CNRS, IJL, F-54000 Nancy, France

[g]Department of Inorgnic Chemistry, Crystallography and Mineralogy. (Unidad Asociada al ICP-CSIC), Faculty of Sciences, University of Malaga, Campus de Teatinos, 29071, Malaga, Spain

[h]Department of Engineering Sciences and Mathematics, Division of Material Science, Luleå University of Technology, Luleå, Sweden

[i]Department of Molecular Sciences and Nanosystems, Ca' Foscari University of Venice, Venezia Mestre, Italy

[j]Nonlinear Dynamics Research Centre (NDRC), Ajman University, P.O. Box 346, United Arab Emirates.

[k]Chemistry Department, College of Science, King Saud University, Riyadh, 11451, Saudi Arabia

*__Corresponding authors__: Alberto Vomiero and Zafar Hussain Ibupoto

Email: zaffar.ibhupoto@usindh.edu.pk

Phone number: +923323129243

Abstract

In this study, we have utilized the raw material of desert gourd fruit juice which distributed in the wide range of desert areas of the world. The desert gourd juice carries a significant content of acidic compounds which can slightly decrease the pH of growth solution, hence it could impart a significant role in the morphological transformation. Also, the purpose of using desert gourd fruit juice was the availability of rich amount of green reducing, capping and stabilizing agents for obtaining the short range and closely packed nanoparticles of $NiCo_2O_4$. The preparation of nanostructured $NiCo_2O_4$ materials was carried out by using desert gourd fruit juice through hydrothermal process followed by thermal annealing in air. The morphology, crystalline structure, surface chemical composition and localized atomic investigations were performed by several analytical techniques. The role of desert gourd fruit juice on the structural and functional features of $NiCo_2O_4$ was also explored. The desert gourd juice through the decrease in the pH of growth solution and carrying green reducing, capping and stabilizing agents originating closely packed $NiCo_2O_4$ nanoparticles instead of nanorod like morphology. The oxygen evolution reaction (OER) half-cell characterization demonstrated overpotential of 260 mV@10 $mAcm^{-2}$, Tafel slope of 62 mV dec^{-1} and durability of 40 hours using $NiCo_2O_4$ nanostructures prepared with 2 mL of desert gourd juice. Moreover, energy storage aspects of $NiCo_2O_4$ nanostructures prepared with desert gourd juice were studied for supercapacitor application and an asymmetric

supercapacitor (ASC) was developed. The findings of presented study revealed a high specific capacitance (Cs) 1958.17 F/g for newly developed ASC and high retention percentage of 99-90% during cycling stability was also notice. The enhanced performance of as prepared $NiCo_2O_4$ nanostructures are attributed from the formation of unique architecture, surface oxygen vacancies, high ionic diffusion, high exposure of surface active sites, fast electron communication, swift charge transport at the interface between electrode and electrolyte.

Keywords: Desert gourd fruit, $NiCo_2O_4$ nanostructures, asymmetric supercapacitor, oxygen evolution reaction

1. Introduction

Renewable energy is the prioritized demand for the current and future needs due to worse situations created by the combustion of fossil fuels towards our environment [1]. Further high utilization of fossil fuels has shown the rapid depletion of their reservoirs around the world [1]. The nonhomogeneous distribution of natural energy reservoirs has induced lots of challenges for the maintenance of peace and harmony on the earth for the survival of human life [2-4]. The combustion of these fossil fuels produces different kind of greenhouse gases like carbon dioxide (CO_2), sulfur dioxide (SO_2), di-nitrogen oxide (N_2O) etc. and they are causing global warming [5]. Hence, new and alternative renewable energy resources like solar, wind and hydro energies with possible uniform utilization throughout the world have been considered a great scientific opportunity for improving human life [1, 6, 7]. For this reason, various renewable energy production methods have been effectively under investigations; among them, water splitting is found to be the best source for the production of high density energy fuel of hydrogen gas [8]. Water splitting is taking place through electrolysis, photo electrochemical and radiolysis for the generation of hydrogen gas fuel [8]. Electrochemical water splitting using electrocatalyst is

highly considered due to its easy processing throughout the 24 hours, production of clean hydrogen fuel and high efficiency. The noble metal-based catalysts like Ru/Ir/Pt/Pd electrocatalysts are the most efficient to date for this kind of technology. However, the limitations of these noble metal-based catalysts are described by their rare abundance in nature, high cost, their half-cell reactions of water splitting and somehow their poor stability in harsh alkaline conditions. [9]. Two half-cell reactions of water splitting are oxygen evolution reaction (OER) at anode, and hydrogen evolution reaction (HER) at cathode [10, 11]. The OER process is the most challenging part of water splitting owing to its difficulty to run efficiently a four electron transfer process, hence it has limited the overall efficiency of water splitting for the production of hydrogen fuel to date [12]. This is the reason a wide range of earth abundant, low cost and scale up nonprecious materials have been studied for the electrochemical water splitting. However the performance of those materials is still not significant to capitalize them for practical applications [13,14]. Furthermore, the obvious availability of sustainable energy resources like wind, water splitting and solar driven technologies has highlighted the need of outperforming energy storage materials and their efficient device configurations [15]. The effective storage of these energy reservoirs inspired the researchers to realize energy storage devices as efficient as possible [16]. The future of these energy storage systems is realized for the applications of electrochemical capacitors and batteries [17]. It has been shown that the energy densities of lithium-ion batteries (LIBs) could achieve a value of 180 $Wh.kg^{-1}$ [18] hence LIBS have limiting and slower power provision. Thus, the use of LIBSs is constrained particularly in energy-storage systems, which are accompanied by the swift and efficient power storage devices; hence they are of immediate need [19, 20]. The electrochemical capacitors are characterized by long cyclic stability, high power density, and accelerated charge-discharge kinetics, inexpensiveness,

therefore they are considered as promising and efficient energy storage devices for a bright future of specific applications [21]. The electrochemical capacitor devices have been categorized into ways first as electric double-layer capacitors (ELDCs) and pseudo capacitors [22-24]. It has been observed that the pseudo capacitors with redox behaviors could give out high energy density [25, 26]. Several potential pseudo capacitive and battery type electrode materials have been investigated [27-35]. Binary metal oxide like nickel-cobalt oxide ($NiCo_2O_4$) with spinel structure has been studied as composite supercapacitors (SCs). In the spinel structure of $NiCo_2O_4$, the tetrahedral and octahedral sites are occupied by Ni, Co atom respectively; hence such structural uniqueness gives the enhanced electrical conductivity to $NiCo_2O_4$ with significant electrochemical activity via Co and Ni metallic ions [36-39].

Beside the development of energy storage electrode materials, there is also hotspot need to fabricate the materials, which can have dual functionality of energy storage and energy conversion. Especially, the electrochemical water splitting, where the design of electrocatalyst has almost the same type of demands to utilize for the strengthening of energy reservoirs. For water splitting, the noble metal based electrocatalysts like RuO_2, IrO_2, and Pt have been found to be the state-of-art catalysts to date. However, their limitations for large scale applications are bound by the rare abundance in nature, and high cost [40]. Various transition metal-based compounds have been studied for both the HER and OER processes [41-44]. The $NiCo_2O_4$ nanostructures have also been explored for OER due to its countable density of active sites, high electron transfer reaction kinetics and mixed oxidation states of Co and Ni [45]. The preparation of $NiCo_2O_4$ by hydrothermal method is scalable, simple, low cost and ecofriendly. These advantages drive $NiCo_2O_4$ to be used for plenty of purposes like electrochemical water splitting and SCs field [46-51]. The synthesis methods have shown impact on the performance of

$NiCo_2O_4$ nanostructured materials, hence different methods have been used to prepare modified and new nanostructures of $NiCo_2O_4$ [52, 53]. Among them, the green approach of using biomass waste has recently received dynamic attention due its cost effectiveness, simplicity, scalability of the synthesis, environment friendliness, and the use of minimum toxic chemicals. For this reason, various biomass wastes have been used during the synthesis of $NiCo_2O_4$ nanostructures [53]. Biomass waste allows the provision of tunable surface of nanostructured materials due to rich natural chemistry of antioxidant and surface modifying agents, which further have demonstrated outstanding functionalities in both water splitting and SCs applications [53]. Among the biomasses, the desert gourd plant fruit juice is also known as desert gourd, colocynth, bitter cucumber, and bitter apple and it is widely spread in deserts of most of the countries in the world [54-56]. Most of the use of desert gourd is taking place in medical applications due its rich medicinal chemistry (see Scheme 1) like carbohydrate, protein, separated amino acid, tannins, saponins, phenolics, flavonoids, flavone glucosides, terpenoids, alkaloids, anthranol, steroids, cucurbitacin, saponin, cardic glycoloids [57, 58]. The existence and the relative percentage of these medicinal compounds in the desert gourd juice are followed by the 7.0% oil, 11.7% protein, 29.5% carbohydrate, and 5.51% dietary fiber content. Linoleic, palmitic oleic, and stearic acids make for 17–23% of the fatty acid composition [59- 61].

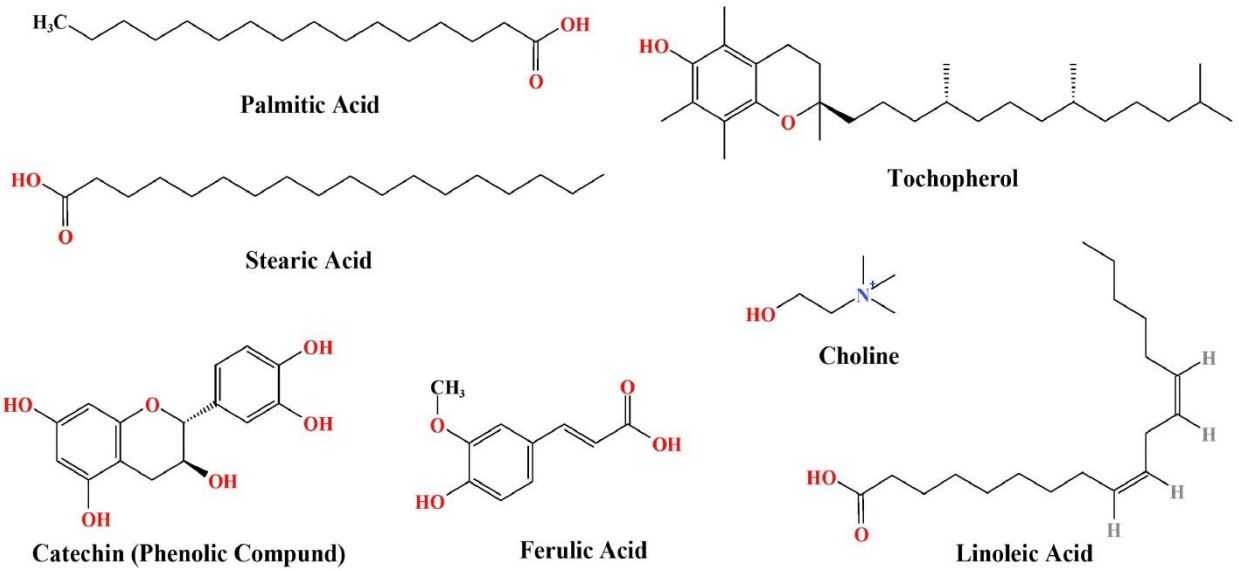

Scheme 1: Molecular structure of various natural product found in desert gourd plant juice.

Many of these compounds have ability to bind effectively with the metal ions and redirecting the morphology into a new shape with increased electrochemical properties [55]. Hence, the purpose of this study was to utilize the green reducing, capping and stabilizing agents from the biomasses like desert gourd. The existence of desert gourd in the desert areas around the world is offering us wide range of useful natural chemicals for the green synthesis of nanostructured materials with enhanced performance. This is the reason, we offer an alternative green, eco and environment friendly approach for the preparation of functional nickel cobalt oxide nanostructures for the energy conversion and storage applications. Furthermore, among the set United Nations (UN) Sustainable Development Goals (SDGs) to minimize the use of hazardous chemicals during the synthesis of materials which become the cause of environmental pollution and at the same time uplift the renewable energy reservoirs. Hence, keeping in view this, the present study offers to avoid the source of toxic chemicals to pollute the environment and the synthesis of functional nanostructured materials for the renewable energy [62, 63]. Furthermore, the desert gourd fruit exhibits unique natural chemistry of antioxidants like fatty acids, proteins, oils and dietary fiber and surface modifying agents like carbohydrates. Therefore, it can be used

potentially to transform the morphology and tune the surface properties of nanostructured materials. The growth process of nanostructured material through rich chemistry of antioxidants kinetically can provide abundant nucleation sites for the well-defined morphology of nanostructured materials with promising functional properties. These attractive features of desert gourd fruit juice motivate us to capitalize it for the structural alteration, tuning the surface properties and producing a unique surface of $NiCo_2O_4$ nanostructures for the efficient energy storage and conversion systems. Such outstanding natural chemistry of antioxidants, surface modifying agents, stabilizing agents and chelating agent groups has not be utilized for the synthesis of $NiCo_2O_4$ nanostructures and their improve electrochemical properties.

In this study, we have investigated the role of desert gourd fruit juice towards the enhancement of electrode material properties of $NiCo_2O_4$ nanostructures using hydrothermal process. The optimization role of desert gourd fruit juice was also done. The $NiCo_2O_4$ nanostructure with 2 mL of desert gourd juice has shown an enhanced OER activity at overpotential of 260 mV @10 $mAcm^{-2}$. Also, the $NiCo_2O_4$ nanostructures prepared with 2 mL of desert gourd juice were used as anode material for the development of asymmetric supercapacitor (ASC), which has shown specific capacitance (Cs) of 1958.17 F/g and high retention percentage of 99-90% of specific capacitance during cycling stability.

2. Experimental Section

2.1. Preparation of $NiCo_2O_4$ nanostructures using desert gourd plant fruit juice by hydrothermal method

Nickel chloride hexahydrate, cobalt chloride hexahydrate, and urea were the chemicals used without further purification to produce bimetallic oxide nanostructures of nickel cobalt oxide ($NiCo_2O_4$). Synthesis of $NiCo_2O_4$ nanostructures was carried out by two processes involving hydrothermal reaction followed by calcination in air as described herein. Before the growth process, desert gourd plant fruit juice was collected by home used juicer machine. Then, growth solution containing volume of 100 mL with equi-molar concentration of 0.1 M each of cobalt chloride hexahydrate and urea with 0.015 M nickel chloride hexahydrate was prepared with uniform dissolution using mechanical stirring. Three beakers of growth solution were taken and in two beakers 1 mL volume (sample 1), and 2 mL volume (sample 2) of desert gourd fruit juice was added respectively. The decrease in the pH of growth solution with addition of 1 mL and 2 mL of desert gourd juice was also found and the corresponded values were as 6. 34 and 5.86 respectively. Third growth solution beaker contained only the precursors of pristine $NiCo_2O_4$ nanostructures with a pH of 6.72. Then, three growth solution beakers of $NiCo_2O_4$ nanostructures were covered with aluminum sheet in order to avoid the evaporation of growth solution. The hydrothermal process was started in the preheated electric oven for 5 hours at 95^oC. After the growth completion, we filtered out the precipitates of hydroxide phase on the ordinary laboratory filter paper and washed them several times with the deionized water. Afterwards, we have dried the precipitates and processed the calcination in air at 500^oC for 5 hours. Then, a black product in powder form was collected and used for further structural and functional investigations. The synthesis process is generalized in scheme 2 for the better visualization of each step of growth process

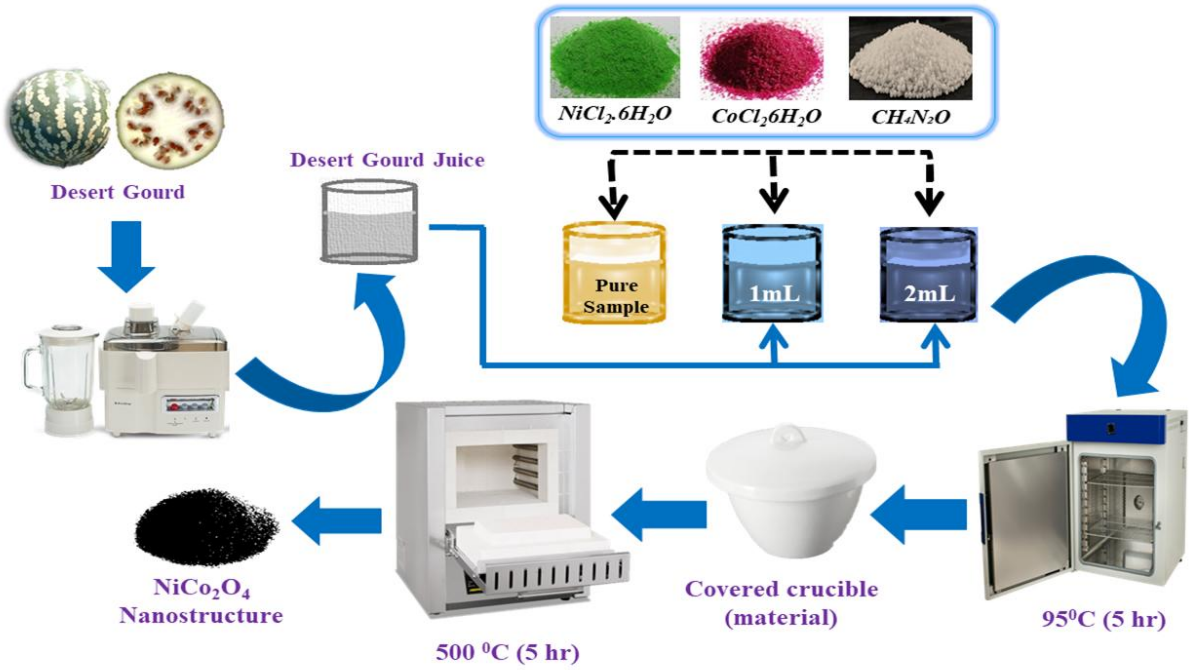

189

190 **Scheme 2:** Desert gourd plant juice assisted synthesis scheme for the synthesis of $NiCo_2O_4$
191 nanostructures

192 The physical characterization was done with respect to morphology, crystalline structure,
193 chemical composition, and surface properties using scanning electron microscope (SEM) with an
194 accelerating voltage of 15 kV, powder X-ray diffraction using X-rays source of wavelength $\lambda_{K\alpha}$
195 = 1.5406 Å from Cu anode material at 45 kV and 46 mA, high resolution transmission electron
196 microscopy (HRTEM) using 200 kV, Tecnai G2 F20, FEI, energy dispersive X-rays
197 spectroscopy (EDX), and X-ray source from Al K_α X-ray resource at 30 eV for the surface
198 analysis using X-ray photoelectron spectroscopy (XPS). The measured binding energies of as
199 prepared materials were compared with the reference binding energy of C1s peak at 284.6 eV.
200 Fourier transform infrared (FTIR) spectra of different nanostructured samples were measured in
201 the range of 500-400 cm^{-1} through the use of Bruker Alfa spectrometer. The sample preparation

of FTIR study was done with the use of small amount of nanostructured sample with KBr to form a pellet and employed for the measurement.

2.2. Electrochemical measurements of desert gourd plant fruit juice derived $NiCo_2O_4$ nanostructures

Two types of electrochemical experiments were performed including OER and supercapacitor characterizations in the alkaline electrolytic conditions. First, OER investigations were done on the surface of different $NiCo_2O_4$ nanostructures using three electrode cell configuration in 1.0 M KOH aqueous electrolyte. For this purpose, working electrode of glassy carbon electrode (GCE) with a diameter of 3 mm was cleaned with alumina paste of 0.3 µM and rubbed by silicon paper followed by washing with the deionized water. The reference electrode was consisting of calomel (Hg/HgO), and graphite rod was used a counter electrode. The modification of GCE was done with $NiCo_2O_4$ nanostructures paste prepared by dissolving 5 mg of each $NiCo_2O_4$ nanostructured sample in 3 mL of deionized water and 100 µL of 5% Nafion binder and sonicated for 10 min. The utilization of 5 µL with a mass of (0.2mg) of each sample paste was dropped onto GCE using drop casting method. Various electrochemical tests were done with different electrochemical modes like linear sweep voltammetry (LSV), cyclic voltammetry (CV), chronopotentiometry and electrochemical impedance spectroscopy (EIS). First, three cycles of CV at low scan rate of 5 mV/s were done followed by three LSV cycles at 2 mV/s. The purpose of using first CV was to stabilize the electrode and to measure well defined half-cell OER signal during the water splitting. Whereas, the EIS was done in the frequency range 100 kHz to 0.01 Hz using amplitude of 10 mV and onset potential of OER to evaluate the charge transfer rate at the interface of electrode material and electrolyte. The non-Faradic CV curves were obtained at

different scan rates to measure the number of active sites involved in the OER process. The durability of optimized electrode material was studied by chronopotentiometry method at a constant current density of 20 mA cm^{-2}. The measured experimental potential against calomel reference electrode was reported herein into reversible hydrogen electrode (RHE) using Nernst equation. Tafel analysis was done to investigate the reaction kinetics with the selected linear part of LSV curves of OER process using Tafel equation and all the OER studies were done at room temperature.

2.3. Asymmetric supercapacitor characterization of desert gourd plant fruit juice derived $NiCo_2O_4$ nanostructures

First supercapacitor studies were done with the three electrode set up then practical aspects were tested with two electrode cell configuration under 3.0M KOH electrolyte conditions.

The chronopotentiometry (CP) was applied to measure the galvanostatic charge-discharge (GCD) curves for the illustration of specific capacitance (C_s) F/g and energy density.

The calculations of C_s, energy density and power density of three electrode cell set up were carried out according to the published work [64].

The used mathematical equations were given as below:

$$C_s = \frac{I \times \Delta t}{m \times \Delta V}$$

Where C_s is the specific capacitance, I the current, Δt the discharge time, ΔV the potential window, *m* the loaded mass on the GCE.

The energy density was calculated as follows [64]

$$E_d = \frac{C_s \times (\Delta V^2)}{2}$$

245 Herein E_d is the energy density, C_s is the specific capacitance, ΔV^2 is the variation in potential.

246 The esitmation of power density is [64]:

$$P_d = \frac{E}{\Delta t}$$

247 where P_d is the power density, E is the energy and Δt is the discharge time.

248 Two electrode set up was used to study the asymmetric supercapacitor device configuration, in
249 which nanostructured $NiCo_2O_4$ was prepared with 2 mL of desert gourd fruit juice as anode and
250 activated carbon (AC) as cathode using 3.0 M KOH electrolyte conditions. The activated carbon
251 slurry was prepared with 15 mg in 3 mL of 99% ethanol and 1 mL of deionized water with
252 volume ratio of (3:1) and 200 µL of 5% Nafion. Uniformly dissolved slurry of AC was achieved
253 by sonication for 15 min. Two GCEs were modified with $NiCo_2O_4$ (sample 2) and AC as
254 positive and negative electrode respectively for the development of asymmetric supercapacitor
255 devices, and they were labeled as $NiCo_2O_4$ DG//AC ASC. The balancing of voltammetric
256 charges for $NiCo_2O_4$ DG (Sample 2) and AC, then loading masses for both electrodes were
257 determined by Q+ = Q– equation as previously reported [65]:

258 $m+ m- = C_s- \Delta V- C_s+\Delta V+$.

259 Whereas: m±, Cs±, and ΔV± represents the mass, C_s, and potential window of $NiCo_2O_4$ DG
260 (Sample 2) (+) and AC (−) electrodes, respectively. The determined value of mass for m+/m−
261 was around 0.17 mg in $NiCo_2O_4$ DG//AC ASC. The total mass (M) used for the calculation of C_s
262 (F g^{-1}), energy density (E, Wh kg^{-1}), and power density (P, W kg^{-1}) was as described and these
263 calculations were done according to the reported work [66]:

$$C_s = \frac{4 \times I \times \Delta t}{m \times \Delta V}$$

Energy density was estimated as below [66]:

$$E_d = \frac{C_s \times (\Delta V^2)}{7.2}$$

Here E_d is the energy density; C_s is the specific capacitance, potential variation ΔV^2

The power density was as obtained by [66]:

$$P_d = \frac{C_s \times 3600}{\Delta t}$$

3. Results and discussion

3.1. Morphology, crystalline, and chemical analysis of various $NiCo_2O_4$ nanostructures derived from desert gourd plant fruit juice

Physical characterization of various samples of $NiCo_2O_4$ nanostructures prepared with and without desert gourd fruit juice in terms of morphology was performed using SEM analysis as shown in Figure 1. The $NiCo_2O_4$ nanostructures without the desert gourd fruit juice confirmed the typical assembled nanorod like morphology as shown in Figure 1(a). The length of each nanorod could be few microns and the sample was found to be heterogeneous in the shape, consisting of aggregated nanoparticles in addition to nanorod. However, the preparation of $NiCo_2O_4$ nanostructures with 1 mL (sample 1) and 2 mL (sample 2) only shown a homogenous morphology of closely packed nanoparticles and the nanorod were lost as shown in Figure 1(b, c). Furthermore, the majority of the compounds of desert gourd juice were acidic in nature and could change the pH of growth of solution; hence such environment of growth solution would

change the morphology due to the etching effect [67-69]. As a consequence, we observed the morphology of closely assembled nanoparticles of $NiCo_2O_4$ as shown in Figure 1(b, c). Furthermore, the presence of green reducing, capping and stabilizing agents in the desert gourd also played role to transform the morphology from nanorod to nanoparticles. The powder XRD was used to measure the diffraction patterns of various $NiCo_2O_4$ nanostructures prepared with the 1mL and 2 mL of desert gourd juice as shown in Figure 1(d). Different XRD diffraction patterns were observed such as 220, 311, 400, 422, 511, 440, and 533 at two theta angle 31.02^o, 36.67^o, 44.66^o, 55.30^o, 58.62^o, 64.95^o, and 77.96^o respectively as shown in Figure 1(d). From XRD analysis, it was found that the diffraction patterns were corresponded to spinel structure and cubic phase of $NiCo_2O_4$ nanostructures and they were well matched the standard JCPDS (card no: 01-080-1542). The XRD study has shown high crystalline properties of as prepared $NiCo_2O_4$ nanostructures.

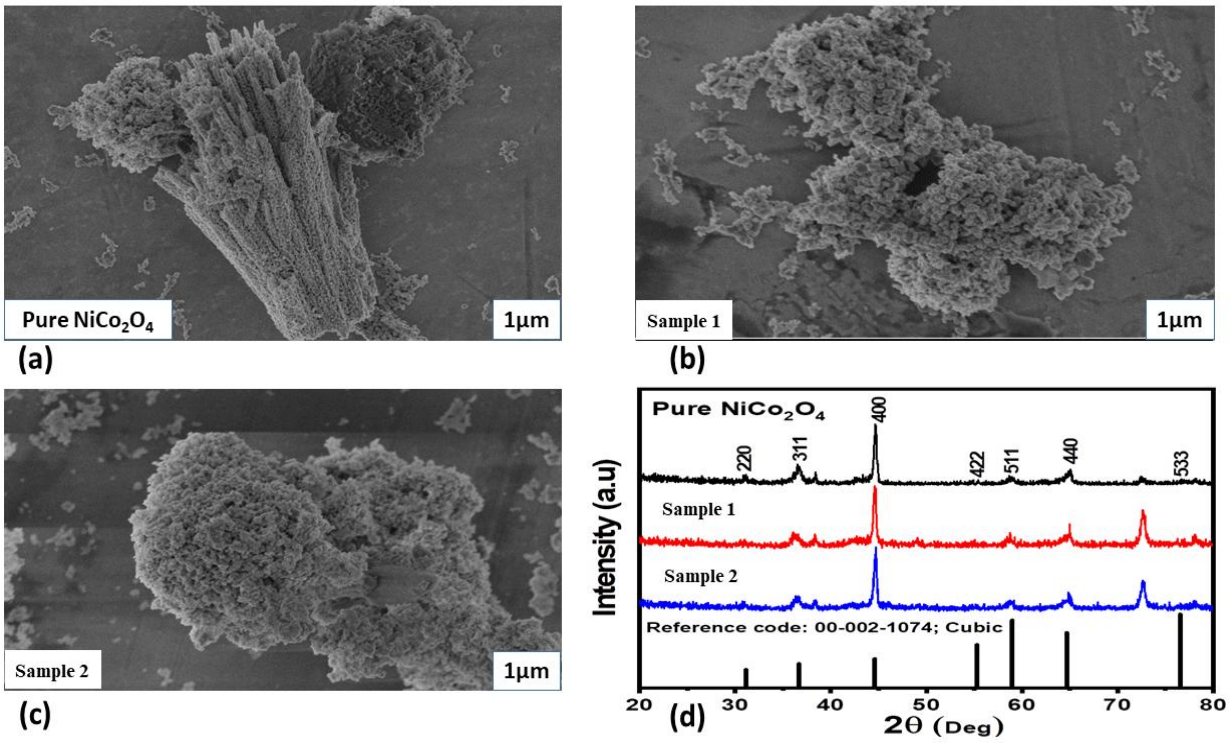

Figure 1: Typical SEM imaging (a) pure $NiCo_2O_4$ nanostructured material, (b, c) $NiCo_2O_4$ nanostructured materials prepared with 1 mL (sample 1) and 2 mL (sample 2) (d) XRD patterns of $NiCo_2O_4$ nanostructured materials prepared with and without desert gourd juice.

Fourier Transform Infra-red (FT-IR) was used to understand the functional groups exhibited by $NiCo_2O_4$ nanostructured materials before and after the thermal annealing process. The FTIR spectra were measured in the range from 4000-500 cm^{-1}, indicating the chemical bonds present in the prepared materials as shown in Supplementary Information (Figure S1a,b). The broad peak at 3557 cm^{-1} corresponded to stretching vibration of hydroxyl groups (-OH) related to non-hydrogen bonded group. Whereas, the peak recorded at 3427 cm^{-1}, suggesting stretching vibration of hydrogen bonded hydroxide group (O-H) [70]. The band peaks observed at 2922 cm^{-1} and 2851 cm^{-1} indicated the C-H vibration bands of CH_2. The peak measured at 2186 cm^{-1} was assigned to atmospheric carbon dioxide as the measurement was done in the air. The peak noticed at 1617 cm^{-1} could be linked to bending vibrations of surface bound water molecules like hydroxyl groups [70, 71]. Most of the metal hydroxide/oxide and spinel structure compounds have stretching bands in the range of 400-700 cm^{-1} [72, 73]. The major peak observed at 570 cm^{-1} could be connected to Ni/Co-O-H bending vibrational modes as shown in Supplementary Information (Figure S1a) [70]. Similarly, FTIR study was performed for the bimetallic oxide phase of $NiCo_2O_4$ prepared with desert gourd juice and almost similar band vibrations were observed, however they were found slightly shifted and with higher intensity, whereas few of the bands were disappeared as shown in Supplementary Information (Figure S1b). Typical bands of Ni-O and C-O vibrations for octahedral and tetrahedral sites were located at 570 cm^{-1} and 661 cm^{-1} respectively [74]. FTIR study did not reveal any functional groups from chemical

316 compounds of the desert gourd juice during the synthesis of $NiCo_2O_4$ using hydrothermal and
317 thermal annealing processes.

318 Scanning transmission electron microscopy (STEM) coupled with energy dispersive X-ray
319 spectroscopy (EDXS), high resolution transmission electron microscopy and selective area
320 electron diffraction (SAED) experiments were carried out to determine the shape, the chemical
321 composition, and the crystallographic structure of pristine $NiCo_2O_4$ and $NiCo_2O_4$ prepared with
322 the use of desert gourd. The pure $NiCo_2O_4$ exhibits a nanorod-like morphology Figure 2(a).
323 These nanorods are constituted of nanoparticles of several tens of nanometers, which are only
324 composed of Ni, Co and O, without any impurities, as shown by STEM-EDXS Figures 2(d-f).
325 Complementary SAED and HRTEM experiments indicate that their crystallographic structure
326 corresponds to the Fd-3m cubic structure of $NiCo_2O_4$ (a = 8.1 Å) Figure 2(c) and insert of Figure
327 2(b).

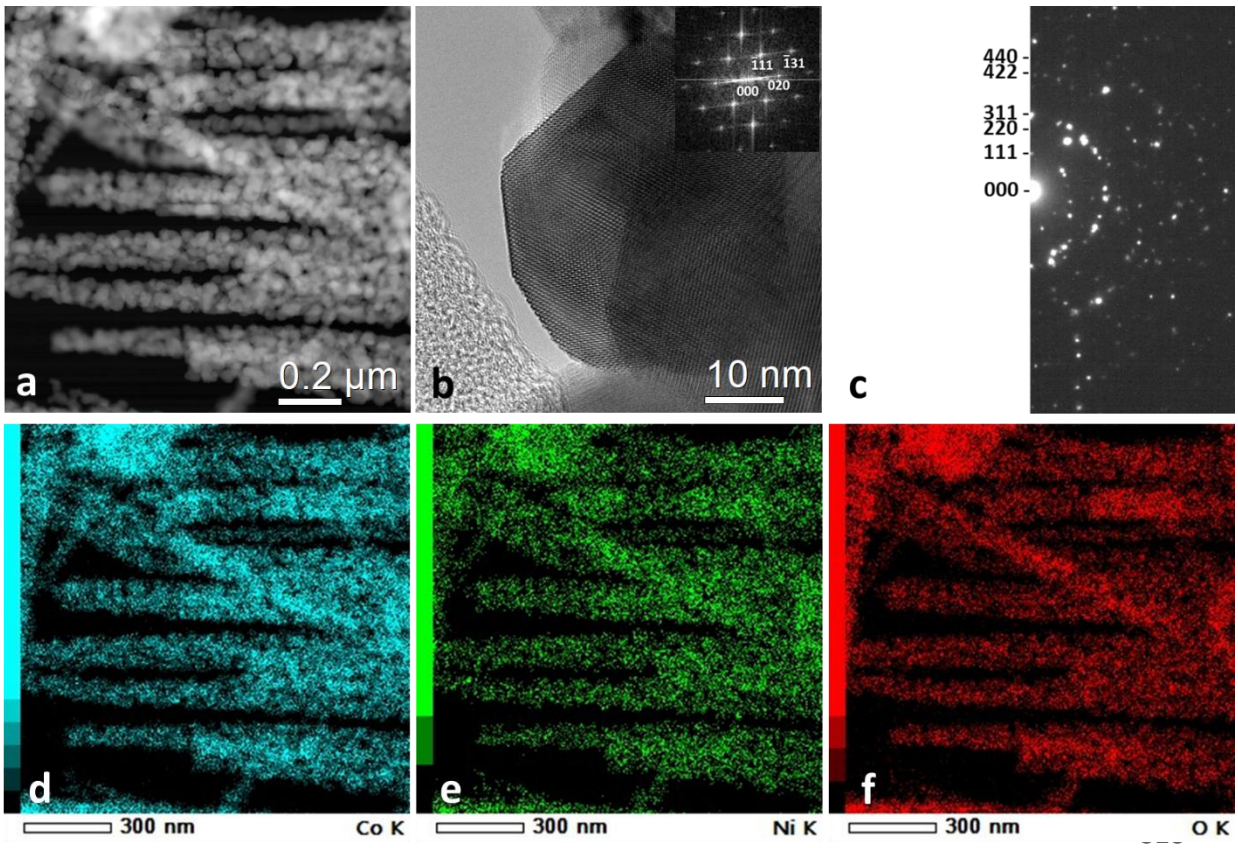

Figure 2: STEM High Angle Annular Dark Field (HAADF) micrograph of pristine $NiCo_2O_4$ (a), HRTEM micrograph of pure $NiCo_2O_4$ (b) with corresponding Fast Fourier Transform (FFT) (insert of b), SAED pattern of pure $NiCo_2O_4$ (c), and corresponding X-maps of cobalt (d), nickel (e) and oxygen (f)

Contrarily to pure $NiCo_2O_4$, $NiCo_2O_4$ prepared with the use of desert gourd sample displays aggregates of nanoparticles of a few tens of nanometers (Figure 3a). These nanoparticles have the same chemical composition as the pristine $NiCo_2O_4$, *i.e.* Ni, Co and O without impurities, as determined by STEM-EDXS (Figures 3d-f). SAED and HRTEM observations evidenced the Fd-3m cubic structure of $NiCo_2O_4$ (Figure 3c and inset of Figure 3b).

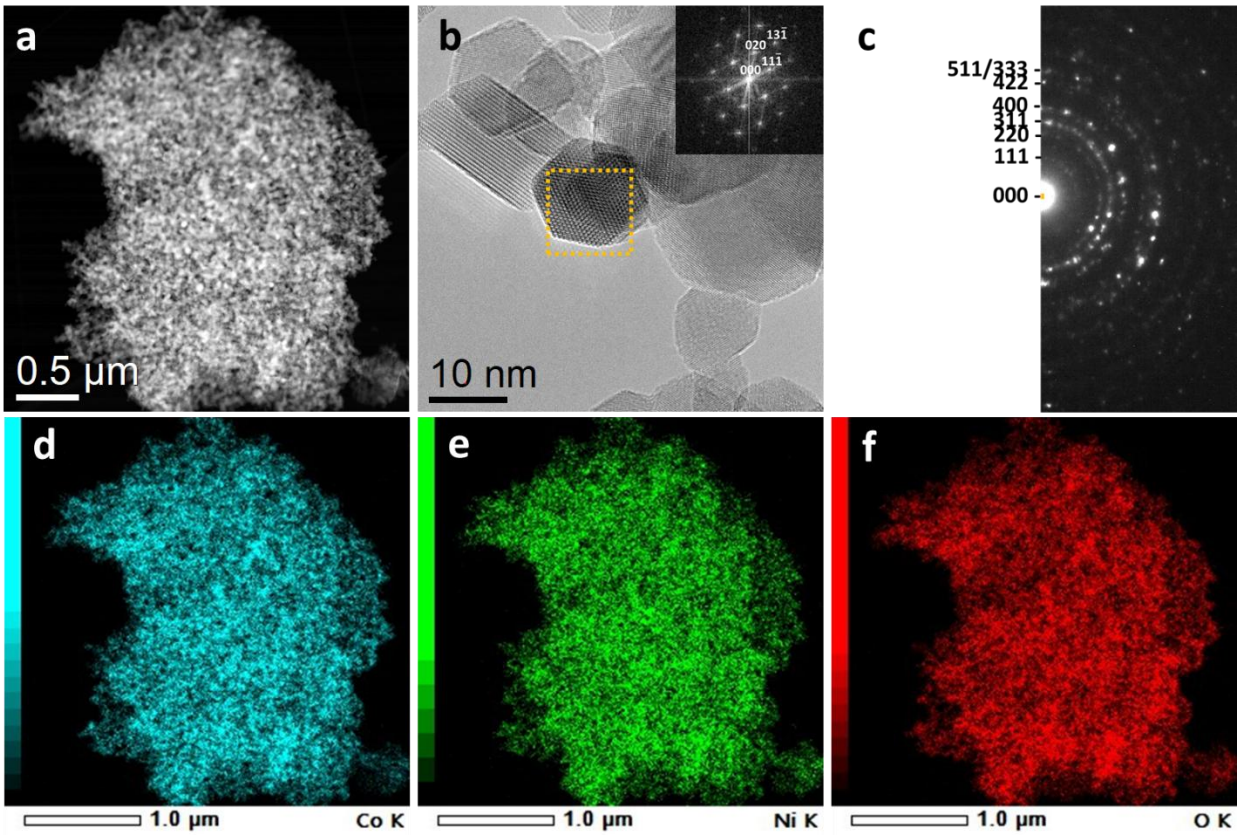

Figure 3: STEM High Angle Annular Dark Field (HAADF) micrograph of $NiCo_2O_4$ prepared with the use of desert gourd (a), HRTEM micrograph of $NiCo_2O_4$ prepared with the use of desert gourd with corresponding Fast Fourier Transform (FFT) of one nanoparticle (yellow dotted square) (insert of b), SAED pattern of $NiCo_2O_4$ prepared with the use of desert gourd (c), and corresponding X-maps of cobalt (d), nickel (e) and oxygen (f)

STEM / HRTEM studies confirmed the high purity of $NiCo_2O_4$ nanostructured material prepared with the use of desert gourd fruit juice; however the nanorod-like morphology of pure $NiCo_2O_4$ was changed into aggregated nanoparticles with the use of desert gourd juice as previously seen form SEM analysis. The HRTEM results of $NiCo_2O_4$ were observed in full agreement with the XRD results. The change in the morphology can further significantly support the surface reaction like in the presented study.

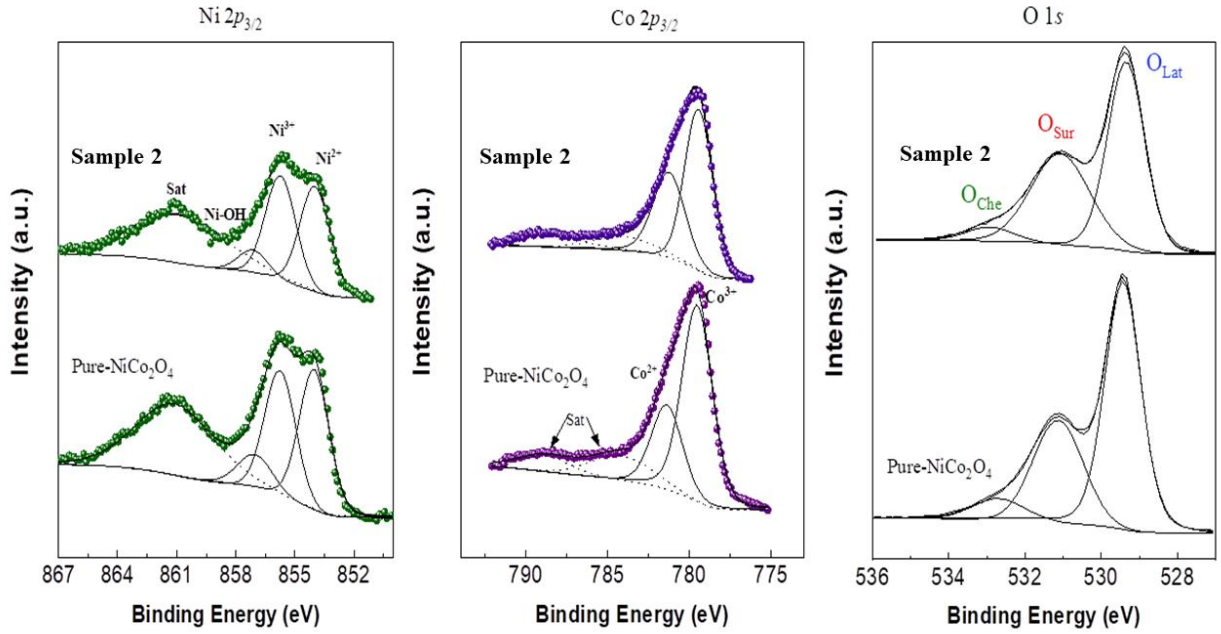

Figure 4: Ni 2p3/2, Co 2p3/2 and O1s spectra of pure $NiCo_2O_4$ and desert gourd assisted grown $NiCo_2O_4$ nanostructures (sample 2).

XPS analysis was used to verify the chemical states and defects on the surface of as grown nanostructured materials as enclosed in Figure 4. The pure $NiCo_2O_4$ and desert gourd derived $NiCo_2O_4$ nanostructures were investigated by XPS and the chemical composition of both samples is only associated with the presence of Co, Ni and O as verified via wide scan survey spectra enclosed in the Supplementary Information (Figure S2). The $Co2p_{3/2}$ signal of pure $NiCo_2O_4$ sample was located at 779.54, 781.39, 784.21 and 788.93 eV and these binding energies for $Co2p_{3/2}$ were found in good agreement with previous work [75]. In the pure $NiCo_2O_4$ sample, the Ni $2p_{3/2}$ peaks were measured at different binding energies (854.03, 855.75, 857.02 and 861.11 eV) and the measured peaks are in good agreement with the previous study

[75]. In the pure sample of pure $NiCo_2O_4$ the variation of the ratio of metal oxidation states (Ni^{2+}/Ni^{3+} and Co^{2+}/Co^{3+}) was quantified as 1.13 and 0.44, respectively.

The $NiCo_2O_4$ sample grown with desert gourd was also analyzed by XPS and the high resolution photoemission signals for $Co2p_{3/2}$ and Ni $2p_{3/2}$ are enclosed in Figure 4. For the $Co2p_{3/2}$ peaks at 779.45, 781.24, 783.96, and 788.44 eV were measured as depicted in Figure 4 [75]. For the Ni 2p3/2, two spin-orbit doublets and shakeup peaks were identified at 853.98, 855.73, 857.13, and 860. 94 eV as enclosed in Figure 4. In the sample of $NiCo_2O_4$ grown with desert gourd, the change in the metallic valence states of nickel and cobalt was also quantified and the corresponding ratio for Ni^{2+}/Ni^{3+} and Co^{2+}/Co^{3+} was found as 1.01 and 0.66 respectively. Overall, in the sample of desert gourd assisted $NiCo_2O_4$, Ni/Co ratio was approximately 0.859. From the high resolution XPS analysis in terms of varied metallic oxidation states, it is revealed that as prepared samples of $NiCo_2O_4$ are well characterized by spinel structure [75]. The surface contamination and defects were also studied via O1s spectra as shown in Figure 4. The O1s spectra is well characterized by three major peaks centered at O1 529.35 eV, O^{-2} at 531.08 eV and O^{-3} 532.69 eV for pure $NiCo_2O_4$ sample. For the $NiCo_2O_4$ synthesized with desert gourd the observed peaks were at O1 529.35, O^{-2} 531.08 and O^{-3} 532.93 eV as shown in Figure 4. Both the samples of $NiCo_2O_4$ carried the typical peaks at 529.43/529.35 eV which are confirming the typical metal–oxygen chemical bond. The surface defects and involvement of any impurity in both the samples was further verified by the appeared peaks at 531.13/531.08 eV and 532.69/532.93 eV as shown in Figure 4. The identified peaks at 531.13/531.08 eV are mainly connected to the relative portion of oxygen vacancies in pure $NiCo_2O_4$ and desert gourd assisted $NiCo_2O_4$ material. However, the peaks at 532.69/532.93eV from both samples are merged due to the chemisorbed oxygenated species [75].

3.2. OER half-cell electrochemical water splitting characterization of $NiCo_2O_4$ nanostructures derived from desert gourd plant fruit juice

The first electrochemical performance of all the prepared samples was explored for OER half-cell water splitting reaction under 1.0M KOH alkaline solutions. For the preliminary OER studies, LSV polarization curves were measured using three electrode cell systems at a scan rate of 2 mV/s as shown in Figure 5(a). The electrochemical performance through LSV curves of three samples of $NiCo_2O_4$ nanostructures was evaluated. The pristine $NiCo_2O_4$ sample has lower activity than the two samples prepared with 1 mL and 2 mL of desert gourd fruit juice in terms of high overpotential of 300 mV at 10 mA cm^{-2}. At the same current density of 10 $mAcm^{-2}$, the overpotential for sample 1 and sample 2 were observed as 280 mV and 260 mV respectively. These OER activities suggest that desert gourd plant juice has lowered the overpotential of 40 mV for the sample 2, offering a new roadmap for the use of abundant natural chemistry source for enhancing the electrochemical activity of nanostructured materials for a particular application. From the overpotential values, it is very much clear that the influence of desert gourd plant fruit juice is highly significant in tuning the electrochemical activity of $NiCo_2O_4$ nanostructures, as shown in Figure 5(a). The performance of sample 2 is indicating the suitability of this new material as an alternative electrocatalyst for the OER half-cell reaction. The linear region of LSV curves was selected to evaluate OER kinetics using Tafel analysis as shown in Figure 5(b). The Tafel slopes of 62 mV dec^{-1}, 72 mV dec^{-1} and 104 mV dec^{-1} were observed for sample 2, sample 1 and pristine $NiCo_2O_4$ nanostructures, respectively. From XPS, analysis, it was found that high amount of higher Co (III) valence states favored the increase in the oxygen vacancies which were further favored the OER activity of optimized sample, this was supported by already existing literature. [76]

The analysis of the Tafel slope indicates that the intrinsic electrochemical properties of $NiCo_2O_4$ were significantly altered by the use of desert gourd plant juice, confirming the variation in the intrinsic features via reduction in size, unique morphology, improved crystalline quality, defects concentration and high density of catalytic sites on the surface. Another accelerated kinetics could be connected to the electron and radical generation during the growth process in the presence of variety of antioxidants from desert gourd plant fruit juice, facilitating the electron transport in $NiCo_2O_4$ nanostructures. Consequently, a favorable OER kinetics was demonstrated, with interesting practical aspects of as prepared $NiCo_2O_4$ nanostructured material. We have also compared the LSV polarization curve obtained after durability test of 40 hours with the LSV curve before the durability measurement, and it was observed that the $NiCo_2O_4$ nanostructures were highly capable in maintaining the onset potential, overpotential and current density again verifying the outstanding stability behavior of $NiCo_2O_4$ nanostructures for long term applications as shown in Figure 5(c). From practical point of view, it is very essential to evaluate the long-term durability of nonprecious electrocatalyst for OER process. For this purpose, we have studied the durability of sample 2 using chronopotentiometry measurement for the time period of 40 hours at a constant current density of 20 mA cm^{-2} as shown in Figure 5(d). Negligible fall in overpotential was observed, suggesting the high durability of the material. It has been shown in the previous studies that the nonprecious $NiCo_2O_4$ nanostructures are stable under low alkaline conditions. To support the observed results of LSV and long-term durability, the double layer capacitance (Cdl) is good indicator to investigate the electrochemical active surface area (ECSA), which describes the exposure of surface active sites during the electrochemical reactions. The ECSA values were calculated for three samples from the non-Faradic region of CV curves measured at different scan rates as shown in Supplementary Information (Figure S3).

It was noticed that sample 2 was accompanied by the highest value of ECSA (13.2 μF cm^{-2}). However, sample 1 and the pure $NiCo_2O_4$ nanostructures exhibited ECSA values of 7.2 μF cm^{-2} and 5.2 μF cm^{-2} respectively; hence sample 2 presented the highest density of active sites, which were exposed during OER process [77]. To study OER reaction kinetics at the interface of electrode material and electrolyte, EIS experiment was performed to evaluate the charge transfer at the interface for the sweeping frequency range from 100 kHz to 0.1 Hz. Previously, it was shown that the semicircle arc at the low frequency region is associated to the charge transfer (R_{ct}) in the Nyquist plots [78, 79] and that a small R_{ct} value validates the fast charge transfer rate [80]. The distinguished Nyquist plots of the three samples were shown in Figure 5(e) and the corresponding Bode plot is reported in Figure 5(f). It can be visualized that the sample 2 exhibited low diameter of semicircle in the fitted EIS data, indicating the swift charge transport at the interface between electrode and electrolyte during OER process [81, 82]. Both the high ECSA and the low charge transfer kinetics contribute to the outstanding electrochemical performance of sample 2 towards an efficient OER half-cell water splitting.

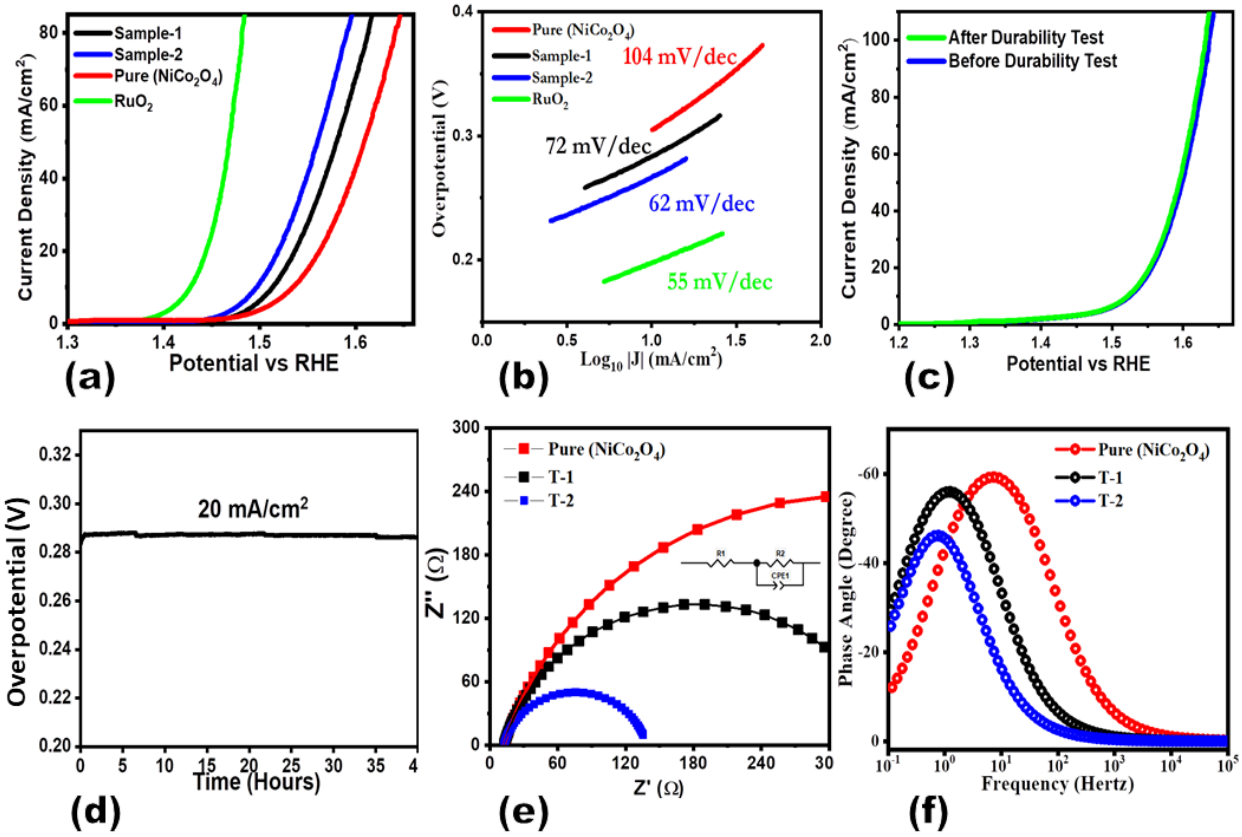

Figure 5: (a) Measured LSV polarization curves for pure $NiCo_2O_4$ nanostructure (sample 1), $NiCo_2O_4$ nanostructure (sample 2) 2 mV/s in 1.0M KOH solution (b) Corresponding Tafel analysis of sample 1, sample 2 and pure $NiCo_2O_4$ (c) Stability of sample 2 (d) Durability for 40 hours at 20 mA cm^{-2} for sample 2. (e) EIS Nyquist plots of sample 1, sample 2 and RuO_2 in the frequency range of 100 kHZ to 0.01Hz using amplitude of 10 mV and onset potential of OER in 1.0M KOH. The inset represents the fitted equivalent circuit. (f) Bode plots of sample 1, sample 2 and RuO_2 from the same EIS.

3.3. Supercapacitor (SC) characterization of $NiCo_2O_4$ nanostructures derived from desert gourd plant fruit juice

The SCs studies were performed on newly prepared $NiCo_2O_4$ nanostructures using desert gourd plant fruit juice using hydrothermal method followed by thermal annealing in air. The desert gourd fruit juice of 1mL and 2 mL were used to understand the role of wide range of natural products in driving the electrochemical performance of $NiCo_2O_4$ nanostructures towards the energy storage application. The electrochemical performance was evaluated by using CV and GCD curves measured in 3.0M KOH electrolyte as shown in Figure 6. The first CV of the pristine sample 1 and sample 2 were measured with different sweeping scan rates for the applied potential range from 0 to 0.5 V as shown in Figure 6(a-c). The CV studies on these samples have shown the Faradic behavior of each material with increasing current densities with the increase of the scan rate. From the redox features of CV curves, the high electrochemical activity within the vicinity of positive potential range is clear, as expected also from previous studies [83, 84]. From CV curves, the redox behavior for each material is almost vanished when going towards the negative potential, indicating the kinetically irreversible phenomenon taking place on the surface of electrode material [85]. The occurrence of oxidation in the forwarding scan, whereas the absence of reduction peak in the reverse scan suggests the existence of irreversible reaction in the presented materials. However, new experimental approaches are needed to better describe the actual mechanism of irreversibility [86]. In the presented CV curves, the drift of the oxidation peak was found in the irreversible process towards higher potential value with increasing value of scan rate because of the overpotential [87]. Interestingly, the shape of CV curves remained unchanged with the increasing sweeping scan rates, confirming an excellent electrical conductivity and outperforming functionality of electrode material toward energy storage application. In the presented study, each material is not fully characterized by perfect pseudo capacitance; however it is closer to battery type material. From CV curves of three

materials, the sample 2 has shown more pronounced battery type behavior as shown in Figure 6(b). The battery type of behavior of sample 2 could be assigned several factors like surface area, ion diffusion rate and conductance of material; hence ECSA and EIS data have shown higher values of catalytic active sites and the charge transfer rate for the sample 2 which favored its battery type behavior. It is shown that the morphology of prepared nanostructured has great role on the battery type behavior as it strongly influence on the value of ion diffusion rate, surface area and electron communication. Sample 2 is has small size nanoparticles which offered high adsorption rate for hydroxide ions, rich exposed catalytic sites and fast charge transfer rate at the interface, hence it behaved like a battery type- material. [88]

Furthermore, the galvanostatic charge-discharge (GCD) curves of pristine $NiCo_2O_4$ nanostructures, sample 1 and sample 2 were measured at applied potential of 0 to 0.5 V using different current densities of 0.8 to 0.94 A g^{-1} as shown in Figure 6(d-f). Each material has demonstrated the triangular shape and symmetric behavior of curves for the selected potential window verifying their significant electrochemical reversibility. The possible reason for the sharp degradation of capacitance for the sample 1 could be only assigned to rapid desorption of ions from the surface of sample 1 which brought a sharp degradation of capacitance.

Some of the slight plateau were noticed in each GCD curve of the three samples, connected to the earlier described CV findings. The linear GCD curves of each electrode material show an excellent population of charges storage throughout the nanostructured $NiCo_2O_4$ materials in aqueous KOH electrolyte. This describes the activating role of various antioxidants and surface modifying agents of desert gourd juice in sample 1 and sample 2, which created multiple ionic channels via well packed and short range nanoparticles, and offered narrow ion and electron channels for the transfer of charge and ionic electrolyte between the electrode material and 3.0M

KOH electrolyte [89, 90]. From GCD curves, it was seen that the discharge time and the capacitance values were linearly decreasing with the increasing current density, which could be attributed to the low penetration of ions into the architecture of the samples because of the swift variation in the potential. The corresponding specific capacitance, energy density, and power density, were calculated from GCD curves as shown in Figure 7. The GCD curves derived values of C_s at 0.8 A g^{-1}, for the pristine sample 1 and sample 2 were found in the order as 197 F/g, 313 F/g, and 435 F/g respectively. Whereas it was observed that C_s was decreasing with the applied current density as shown from GCD curves behavior Figure 7(a). Moreover, during the measured cycling stability GCD curves for the pure $NiCo_2O_4$ nanostructures, sample 1 and sample 2, the obtained values of columbic efficiency and capacitance retention percentage were found as 52%/88-60%, 66%/110-80%, and 74%/103-93% respectively as shown in Figure 7(b). Also, the cycling stability was studied to verify the columbic efficiency of 66%, 74% and 52% for the sample 1, sample 2 and pure $NiCo_2O_4$ nanostructures, respectively, as shown in Figure 7(c). Furthermore, the energy density and power density were observed in the order for 4.15 Wh/Kg^{-1}/155.60 W/Kg, 6.31 Wh/Kg^{-1}/152.40 W/Kg, 9.53 Wh/Kg^{-1}/158.84 W/Kg at 0.8 A g^{-1} for pristine $NiCo_2O_4$ nanostructures, sample 1 and sample 2 respectively as shown in Figure 7(d-f). The observation about the energy density indicates that it depends on the C_s, which is further highly dependent on the applied current density; hence we have used smaller values of energy density compared to the reported works where various researchers have used high applied current density. Our obtained values of C_s for sample 1 and 2 are either superior or equal to many of the recently reported $NiCo_2O_4$ nanostructures-based electrode materials [91-93] under the low applied energy density values. Importantly, the obtained GCD curves for each electrode material exhibited capacitive features due to close triangular shape with well-defined capacitive

properties and a Faradic aspect owing to the negligible plateau look of each GCD curve. Furthermore, the performance evaluation of three electrodes based supercapacitor is summarized in Table (S1).

The structural analysis has shown that the optimized sample was characterized with small nanoparticles of few tens nm as confirmed by STEM/HRTEM which are in good agreement with SEM results. The small size of nanoparticles offers the large exposure to electrolytic ions for the adsorption; hence favorable electrochemical performance was noticed for the optimized sample. Furthermore, the optimized sample exhibited high amount Co(III) ions which induced high surface oxygen vacancies on the surface of optimized $NiCo_2O_4$ nanostructures prepared with desert gourd juice, consequently improved electrochemical supercapacitor and OER performance was observed. The optimized $NiCo_2O_4$ nanostructures with rich surface oxygen vacancies have offered the more adsorption of hydroxide ions which are the reactive species for the charge storage and oxygen production. The electrochemical studies about the active surface sites for the frequent interaction of electrolytic ions and fast charge transfer at the interface together played dynamic role for the enhanced electrochemical activity of optimized sample.

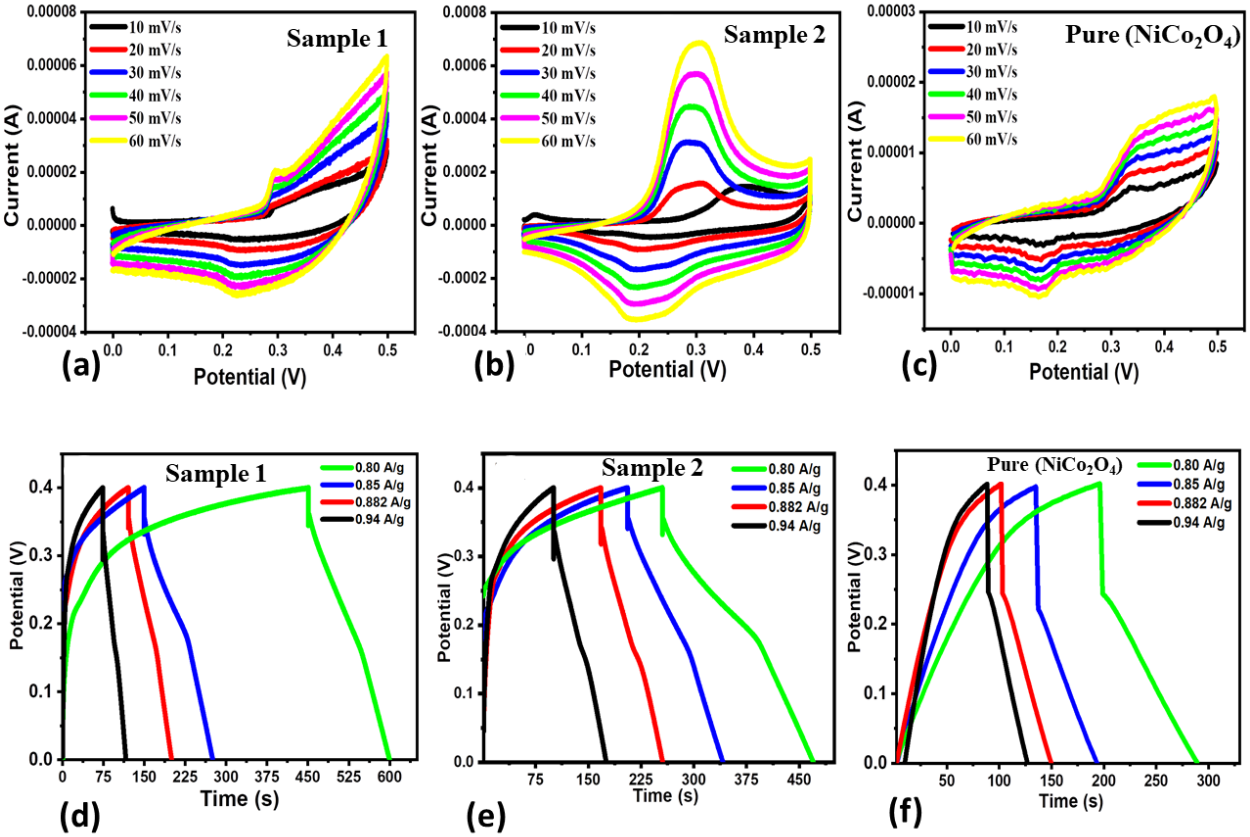

Figure 6: (a-c) Different CV curves at various scan rates in 3.0M KOH for sample 1, sample 2, and pure $NiCo_2O_4$ nanostructure (d-f) corresponding GCD curves of for sample 1, sample 2 and pure $NiCo_2O_4$ nanostructure in 3.0M KOH at different 0.8, 0.85, 0.88, and 0.94 A g^{-1}.

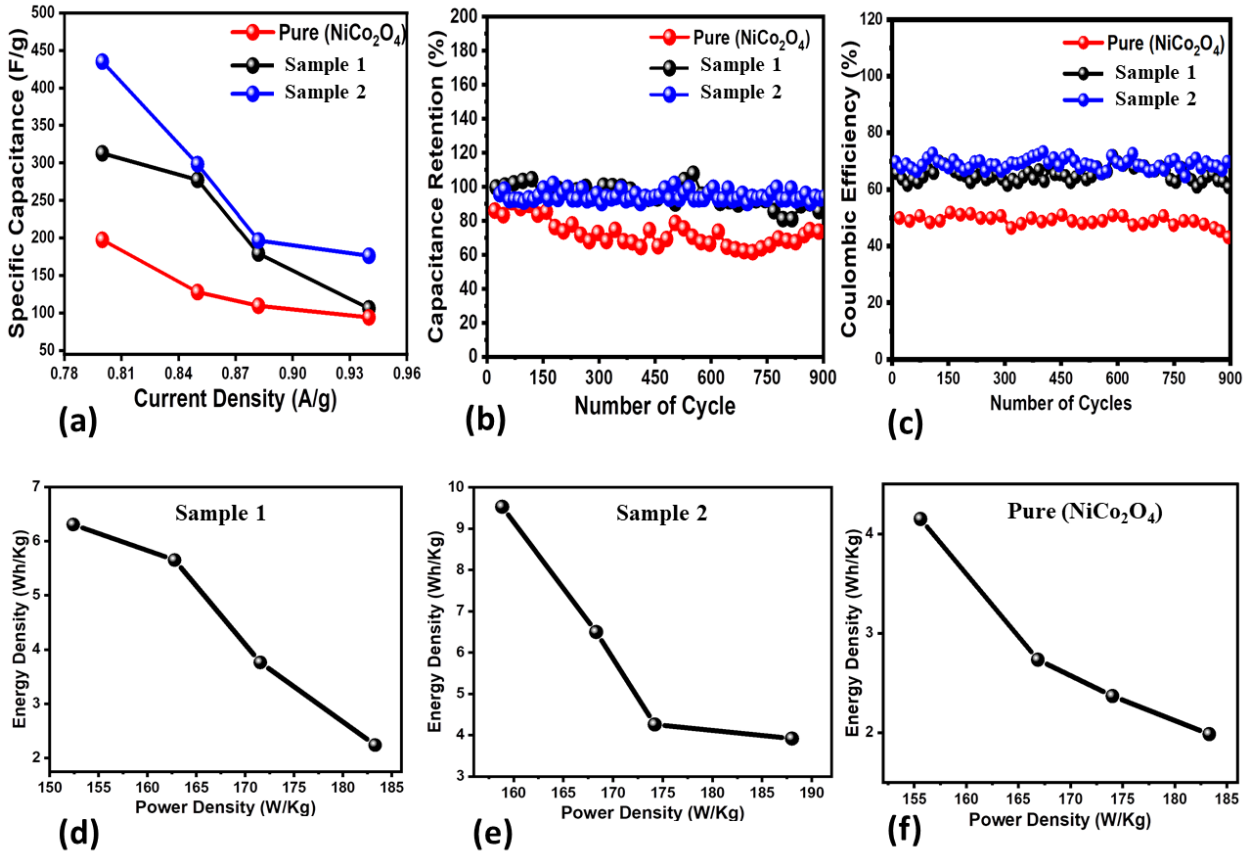

Figure 7: (a) Specific capacitance (C_s) of sample 1, sample 2 and pure $NiCo_2O_4$ (b) percentage retention specific capacitance during cycling stability for sample 1 and sample 2, estimated from GCD curves. (c) Columbic efficiency sample 1, sample 2, and pure $NiCo_2O_4$ cycling stability of GCD curves (d-f) Corresponding energy density of sample 1, sample 2 and pure $NiCo_2O_4$, respectively.

At the same time, three electrode supercapacitor application of as activated carbon (AC) was studied by CV curves and GCD curves as shown in Supplementary Information (Figure S4). The pure AC has shown non-Faradic behavior and with limited specific capacitance as shown by CV curves in Figure S4 (a). The GCD curves have shown triangular shape as shown in Figure S4 (b), with a specific capacitance value of 261 F/g and the energy density of 5.7 Wh/kg, indicating the

poor energy and capacitance for the development of energy storage device as shown in Figure S4 (c-d). Moreover, the calculated the values of C_s, energy density and power density for AC in the three electrode cell set up are given in Table (S1).

3.4. Asymmetric Supercapacitor (ASC) characterization

After understanding the electrochemical performance of pristine $NiCo_2O_4$ nanostructures, sample 1 and sample 2, we have optimized electrode material, which was further assembled as practical positive electrode with negative electrode of activated carbon (AC) towards the development asymmetric supercapacitor (ASC) device. The representation of two electrode cell asymmetric supercapacitor is described $NiCo_2O_4$ DG//AC ASC. Figure 8 shows the CV curves at different scan rates and GCD curves at various applied current density of two electrode configuration. Figure 8(a) shows the CV curves at scan rates from 10 to 110 mV/s and with increasing of scan rate the CV curves were found to be slightly changed in the shape, suggesting the favorable electrochemical reaction on the surface of electrode materials and reversibility. Figure 8(b) shows the typical triangular shape of GCD curves without plateau at different current density ranging from 0.8 to 0.94A g^{-1}, revealing highly reversible redox processing in the developed ASC device. Importantly, the 84% C_s initially was retained at a 0.8 Ag^{-1} confirming an excellent kinetics activity of the ACS device. These obtained values of high C_s and electrochemical activity rate offered potential and promising features for the presented $NiCo_2O_4$ DG//AC ASC device for practical uses. Figure 8(c) describes the C_s retention percentage about 99-90% during the 900 GCD cycles measured for cycling stability, suggesting that ASC device is potentially associated with long-term retaining of C_s. The specific capacitance (C_s) was estimated from the GCD curves. The value of Cs of (1958.17 F/g) was observed higher at low current density. However, at the higher current densities such as 0.85, 0.88 and 0.94 Ag^{-1} the Cs values were

estimated 1948.87 F/g, 1688.55 F/g and 1654.32 F/g respectively as shown in Figure 8(d). Moreover, the energy density and power density are also useful aspects of ASC device for real performance evaluation. Therefore, they were calculated from GCD curves at 0.8 Ag^{-1} and found as energy density 41 Wh/Kg, and power density of 620 W/Kg as shown in Figure 8(e). The energy density of $NiCo_2O_4$ DG//AC ASC device is still far better than the recently reported ASC devices such as WC/CuO//WC (13.6 $Wh.kg^{-1}$ at 350.3 W kg^{-1}) [94] etc. Furthermore, the columbic efficiency was also evaluated and retained by 96-82% for 900 GCD cycles as shown in Figure 8(f), which is also an efficient indicator for the practical aspects of as designed ASC device. Based on the structural, chemical composition, morphology, surface properties, the sample 2 was found to be highly active owing to its high density of active sites for reversible redox process from short range nanoparticles of $NiCo_2O_4$, low charge transfer resistance, swift electron and ionic transfer kinetics, higher electrical conductivity of material, consequently high performance electrochemical performance was demonstrated by sample 2.

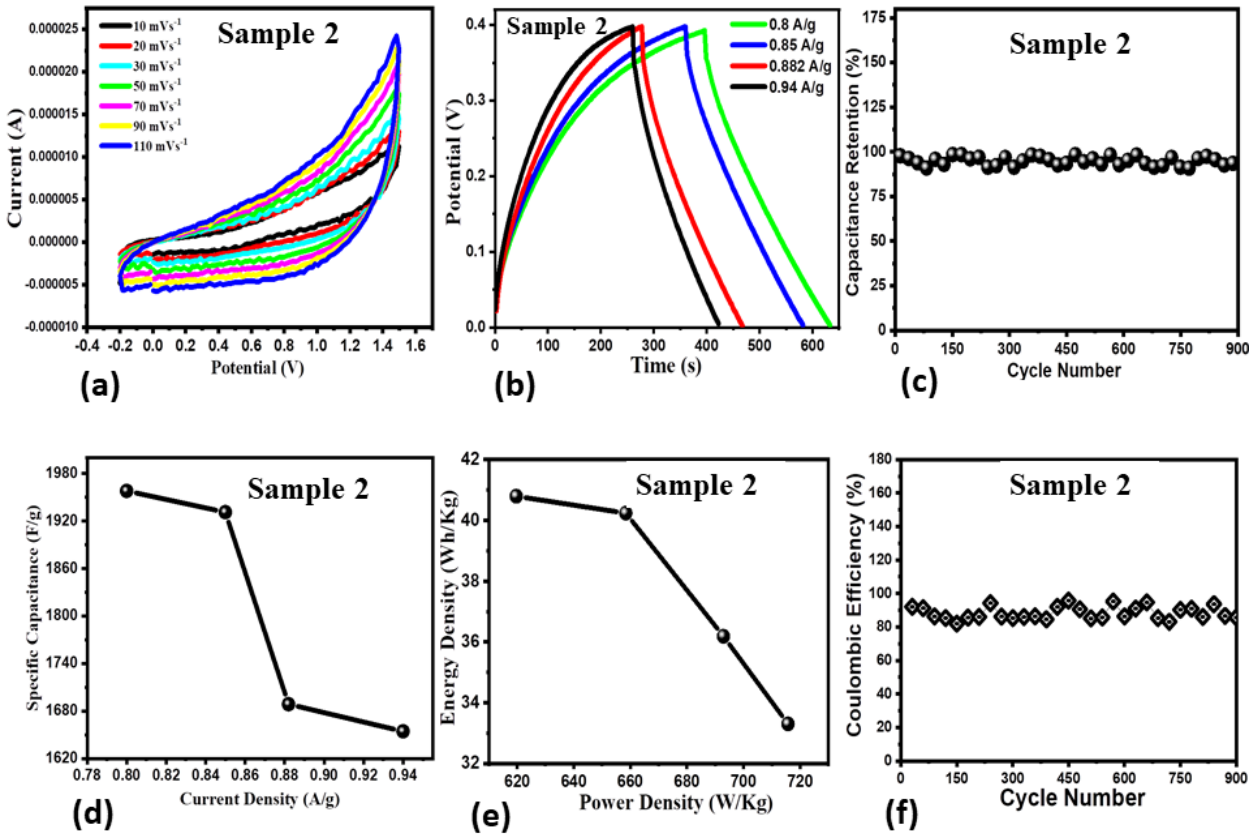

590

591 **Figure 8:** (a) Measured CV curves of (sample 2) at various scan rates in 3.0M KOH. (b) GCD
592 curves at various 0.8, 0.85, 0.88, and 0.94 Ag^{-1} of (sample 2). (c) Cycling stability from GCD
593 curves at $0.8Ag^{-1}$ of (sample 2). (d) Specific capacitance of (sample 2) from GCD curves. (e)
594 Energy density of (sample 2). (f) Columbic efficiency of (sample 2) during cycling stability of
595 GCD curves in 3.0M KOH.

596

597

598

599

Table 1: Measured indicators for asymmetric supercapacitor using two electrode configuration of $NiCo_2O_4$ nanostructure (sample 2) for practical applications

Sample	Current Density (A/g)	Specific capacitance (F/g)	Energy density (Wh/kg)	Power Density (W/kg)	Columbic Efficiency %	Capacitance Retention %
Sample 2	0.8	1958	41	620	96-82%	99-90% (900 Cycles)
	0.85	1949	41	658		
	0.882	1689	36	693		
	0.94	1654	33	716		

Overall, enhanced electrochemical activity of $NiCo_2O_4$ nanostructures prepared with desert gourd plant fruit juice (sample 1 and sample 2 respectively), pristine sample, RuO_2 in terms of overpotential at 10 and 50 mA cm^{-2}, Tafel slope values, specific capacitance and energy density is described by bar graphs in Supplementary Information (Figure S5). Furthermore, the performance of $NiCo_2O_4$ nanostructures prepared with desert gourd plant fruit juice (sample 2) was compared with the recently reported $NiCo_2O_4$ based electrode material as given in Table (S3). It is obvious that the presented material has equal or superior performance of energy density and specific capacitance, when compared with the high applied energy density in the reported works compared to the present work. Moreover, the OER performance of sample 2 was also compared with the recently reported electrocatalysts in term of overpotential as given in Table (S4). It is obvious that the presented material has equal or better performance in terms of synthesis, cost-effectiveness, simplicity, low overpotential and ecofriendly nature.

4. Conclusions

In summary, we have used the desert gourd fruit juice as a raw biomass material, which is possessing high density of green natural compounds with properties like reducing, capping and stabilizing agents. They have effectively changed the morphology $NiCo_2O_4$ nanostructures and surface properties during the hydrothermal process followed by thermal combustion in air. The morphology, surface oxygen vacancies and relative ratio of metal oxidation states was quantified. The $NiCo_2O_4$ nanostructures prepared with 2 mL of desert gourd juice has shown drastic lowering of overpotential of 260 mV@10 mA cm^{-2}, and Tafel slope of 62 mV dec^{-1} during OER process. Moreover, the energy storage functionality of as prepared $NiCo_2O_4$ nanostructures with desert gourd juice was also evaluated through three and two electrode configurations. The realization of asymmetric supercapacitor was described by specific capacitance (C_s) 1958 F/g and retention percentage of 99-90% during cycling stability. The presented study strongly suggests the utilization of raw functional materials form the desert with unique natural chemistry, which can potentially alter the morphology and surface properties of new generation of high-performance electrode materials for the strengthening of energy storage and conversion applications.

Acknowledgments

The authors extend their sincere appreciations to Researchers Supporting Project number (RSP2023R79), King Saud University, Riyadh, Saudi Arabia, for partial funding of this work. B.V. and E.M would like to also thank the platform “Microscopies, Microprobes and Metallography (3M)” at the Institut Jean Lamour (IJL, Nancy, France) for TEM and SEM facilities.

Conflict of Interest Authors declare no conflict of interest in this study

5. References

[1] J.E. Lee, K.J. Jeon, P.L. Show, S.C. Jung, Y.J. Choi, G.H. Rhee, K.Y. Lin, Y.K. Park,. Mini review on H2 production from electrochemical water splitting according to special nanostructured morphology of electrocatalysts. Fuel. Jan (2022) 15 308:122048.

[2] G. Centi, S. Perathoner, Chemistry and energy beyond fossil fuels. A perspective view on the role of syngas from waste sources, Catalysis. Today 342 (2020) 4-12.

[3] K. Nagy, K. Körmendi, Use of renewable energy sources in light of the New Energy Strategy for Europe 2011–2020, Applied Energy 96 (2012) 393-399.

[4] Tolón-Becerra A, Lastra-Bravo X, and Bienvenido-Bárcena F. Proposal for territorial distribution of the EU 2020 political renewable energy goal, Renewable. Energy 36 (2011) 2067-2077.

[5] L. Suganthi, A. Williams, Renewable energy in India—a modelling study for 2020–2021, Energy. Polic 28 (2020) 1095-1109.

[6] J. Lowitzsch, C.E. Hoicka, and F.J. van Tulder, Renewable energy communities under the 2019 European Clean Energy Package–Governance model for the energy clusters of the future?. Renewable and Sustainable Energy Reviews 122 (2020) 109489.

[7] A. Qazi Towards sustainable energy: a systematic review of renewable energy sources, technologies, and public opinions, IEEE. access 7 (2019) 63837-63851.

[8] M.N. Dudin, E.E. Frolova, O.V. Protopopova, O. Mamedov, and S.V Odintsov, Study of innovative technologies in the energy industry: nontraditional and renewable energy sources. Entrepreneurship and Sustainability 6 (2019) 1704-20.

[9] Y. Zhou, H.J Fan. Progress and challenge of amorphous catalysts for electrochemical water splitting. ACS Materials. Letters 3 (2020) 136-147.

[10] L. Li, P Wang, Q. Shao, X. Huang, Metallic nanostructures with low dimensionality for electrochemical water splitting, Chemical Society Reviews 49 (2020) 3072-3106.

[11] K. Ham, Hong, S Kang, K Cho, J Lee, Extensive active-site formation in trirutile $CoSb_2O_6$ by oxygen vacancy for oxygen evolution reaction in anion exchange membrane water splitting . ACS Energy Letters 6 (2021) 364-370.

[12] C. Li, J.B. Baek, Recent advances in noble metal (Pt, Ru, and Ir)-based electrocatalysts for efficient hydrogen evolution reaction. ACS omega 5 (2019) 31-40.

[13] T. Reier, M. Oezaslan, P. Strasser, Electrocatalytic oxygen evolution reaction (OER) on Ru, Ir, and Pt catalysts: a comparative study of nanoparticles and bulk materials. Acs Catalysis 2 (2012) 1765-1772.

[14] Z.P. Wu, X.F. Lu, S.Q. Zang, X.W. Lou, Non-noble-metal-based electrocatalysts toward the oxygen evolution reaction, Advanced Functional Materials 30 (2020) 1910274.

[15] X. Lin, Y. Wang, M. Zou, T. Lan, Y. Ni, Electrochemical non-enzymatic glucose sensors based on nano-composite of Co_3O_4 and multiwalled carbon nanotube. Chinese Chemical Letters 30 (2019) 1157-1160.

[16] D. Zhao, H. Liu, X. Wu, Bi-interface induced multi-active MCo_2O_4@ MCo_2S_4@ PPy (M= Ni, Zn) sandwich structure for energy storage and electrocatalysis. Nano Energy 57 (2019) 363-370.

[17] C.W. Peng, Cobalt phosphate nanoparticles decorated with nitrogen-doped carbon layers as highly active and stable electrocatalysts for the oxygen evolution reaction. Chin. Chem. Lett. 23 (2019) 420-35.

[18] Y. Li, L. Hu, W. Zheng, X Peng, M. Liu, P.K. Chu, L.Y. Lee, Ni/Co-based nanosheetarrays for efficient oxygen evolution reaction. Nano Energy 52 (2018) 360-368.

685 [19] N. Iqbal, Highly flexible $NiCo_2O_4$/CNTs doped carbon nanofibers for CO_2 adsorption
686 and supercapacitor electrodes. J. Colloid Interface Sci 30 (2016) 368-82
687 [20] Y.Q. Wu, Sol-gel approach for controllable synthesis and electrochemical properties of
688 $NiCo_2O_4$ crystals as electrode materials for application in supercapacitors. Electrochim.
689 Acta 53 (2011) 534-58.
690 [21] J. Pu, J. Wang, X. Jin, F. Cui, E. Sheng, Z. Wang, Porous hexagonal $NiCo_2O_4$ nanoplates
691 as electrode materials for supercapacitors. Electrochimica Acta 106 (2013) 226-234
692 [22] D. Lei, X.D. Li, M.K. Seo, M.S. Khil, H.Y. Kim, B.S. Kim, $NiCo_2O_4$ nanostructure-
693 decorated PAN/lignin based carbon nanofiber electrodes with excellent cyclability for
694 flexible hybrid supercapacitors. Polymer 132 (2017) 31-40.
695 [23] M. Yu, J. Chen, Y. Ma, J. Zhang, J Liu, S Li, J. An, Hydrothermal synthesis of $NiCo_2O_4$
696 nanowires/nitrogen-doped graphene for high-performance supercapacitor. Applied
697 surface science 314 (2014) 1000-1006
698 [24] B.R. Wiston, Electrochemical performance of hydrothermally synthesized flower-like
699 alpha-nickel hydroxide. Vacuum 45 (2019) 787-94
700 [25] H.Q. Liu, Ternary core-shell structured transition metal chalcogenide for hybrid
701 electrochemical capacitor. Chin. Chem. Lett. 20 (2018) 8620-36.
702 [26] K.L. Yan, X. Shang, Z. Li, B. Dong, X. Li, W.K. Gao, J.Q. Chi, Y.M. Chai, C.G. Liu,
703 Ternary mixed metal Fe-doped $NiCo_2O_4$ nanowires as efficient electrocatalysts for
704 oxygen evolution reaction. Applied Surface Science (2017) 416:371-378
705 [27] R Chen, H.Y Wang, J. Miao, H. Yang, B. Liu, A flexible high-performance oxygen
706 evolution electrode with three-dimensional $NiCo_2O_4$ core-shell nanowires. Nano Energy
707 11 (2015)333-340

[28] W. Jiang, F. Hu, S. Yao, Z. Sun, X. Wu, Hierarchical $NiCo_2O_4$ nanowalls composed of ultrathin nanosheets as electrode materials for supercapacitor and Li ion battery applications. Materials Research Bulletin (2017) 303-309.

[29] Y. Zhao, X. Zhang, J. He, L Zhang, M. Xia, F. Gao, Morphology controlled synthesis of nickel cobalt oxide for supercapacitor application with enhanced cycling stability. Electrochimica Acta 174 (2015) 51-56.

[30] W. Liu, J. Bao, L. Xu, M. Guan, Z. Wang, J. Qiu, Y. Huang, J. Xia, Y. Lei, H. Li, NiCo2O4 ultrathin nanosheets with oxygen vacancies as bifunctional electrocatalysts for Zn-air battery. Applied Surface Science 478 (2019) 552-559.

[31] Liang HW, Wu ZY, Chen LF, Li C, and S.H. Yu. Bacterial cellulose derived nitrogen-doped carbon nanofiber aerogel: An efficient metal-free oxygen reduction electrocatalyst for zinc-air battery. Nano Energy 11 (2015) 366-376.

[32] J. He, Y. Zhao, D.B. Xiong, W Ran, J. Xu, Y. Ren, L Zhang,Y. Tang, F. Gao, Biotemplate assisted synthesis of 3D hierarchical porous NiO for supercapatior application with excellent rate performance. Materials Letters 128 (2014) 117-120.

[33] F. Zheng, C. Xi, J. Xu, Y. Yu, W. Yang, P Hu,Y. Li, Q. Zhen, S. Bashir, J.L. Liu. Facile preparation of WO_3 nano-fibers with super large aspect ratio for high performance supercapacitor. Journal of Alloys and Compounds 772 (2019) 933-942.

[34] Z. Shi, L Xing, Y. Liu, Y. Gao J. Liu, A porous biomass-based sandwich-structured Co_3O_4@ Carbon Fiber@Co_3O_4 composite for high-performance supercapacitors. Carbon 129 (2018) 819-825.

[35] Y. Zhao, Z. Wang, R. Yuan, Y. Lin, J. Yan, J. Zhang, Z. Lu, D. Luo, J. Pietrasik, M.R Bockstaller, K. Matyjaszewski, ZnO/carbon hybrids derived from polymer

nanocomposite precursor materials for pseudocapacitor electrodes with high cycling stability. Polymer 137 (2018) 370-377.

[36] J. Han, M. Wang, Y. Hu,C. Zhou, R. Guo, Conducting polymer-noble metal nanoparticle hybrids: Synthesis mechanism application. Progress in Polymer Science 70 (2017) 52-91.

[37] S. Sun, T. Zhai, C. Liang, S.V. Savilov, H. Xia, Boosted crystalline/amorphous $Fe_2O_{3-\delta}$ core/shell heterostructure for flexible solid-state pseudocapacitors in large scale. Nano Energy 45 (2018) 390-397.

[38] C. Xia, W. Chen, X. Wang, M. N. Hedhili, N Wei, H. N. Alshareef, Highly stable supercapacitors with conducting polymer core- shell electrodes for energy storage applications. Advanced Energy Materials 5(8) (2015 1401805.

[39] C. Zhu, D. Wen, S. Leubner, M. Oschatz, W. Liu, M. Holzschuh, F. Simon, S. Kaskel, A. Eychmüller, Nickel cobalt oxide hollow nanosponges as advanced electrocatalysts for the oxygen evolution reaction. Chemical communications 51 (2015) 7851-7854.

[40] J. Jiang, A. Zhang, L. Li, L. Ai, Nickel–cobalt layered double hydroxide nanosheets as high-performance electrocatalyst for oxygen evolution reaction. Journal of Power Sources 278 (2015) 445-451.

[41] A. Eftekhari, Tuning the electrocatalysts for oxygen evolution reaction. Materials Today Energy 5 (2017) 37-57.

[42] T. Noor, L. Yaqoob, N. Iqbal, Recent advances in electrocatalysis of oxygen evolution reaction using noble-metal, transition-metal, and carbon-based materials. ChemElectroChem 8 (2021) 447-483.

[43] G.H. Moon, M. Yu, C.K. Chan, H. Tüysüz, Highly Active Cobalt- Based Electrocatalysts with Facile Incorporation of Dopants for the Oxygen Evolution Reaction. Angewandte Chemie. 131 (2019) 3529-3533.

[44] F. Song, L. Bai, A. Moysiadou, S. Lee, C. Hu, L. Liardet, X. Hu, Transition metal oxides as electrocatalysts for the oxygen evolution reaction in alkaline solutions: an application-inspired renaissance. Journal of the American Chemical Society 140(25) (2018) 7748-7759.

[45] F. di Lena, K. Matyjaszewski, Transition metal catalysts for controlled radical polymerization. Progress in Polymer Science 35 (2010) 959-1021.

[46] N. W. Kinzel, C. Werlé, W. Leitner, Transition metal complexes as catalysts for the electroconversion of CO_2: an organometallic perspective Angewandte Chemie International Edition. 60 (2021) 11628-11686.

[47] H. Sun, V. Yan, F. Liu, W. Xu, F. Cheng, J. Chen, Self-supported transition-metal-based electrocatalysts for hydrogen and oxygen evolution. Advanced materials 32 (2020) 1806326.

[48] A. Sivanantham, P. Ganesan, S. Shanmugam, Hierarchical $NiCo_2S_4$ nanowire arrays supported on Ni foam: an efficient and durable bifunctional electrocatalyst for oxygen and hydrogen evolution reactions, Advanced Functional Materials 26 (2016) 4661-4672.

[49] J. Liu, J. Ma, Z. Zhang, Y. Qin, Y. J. Wang, Y. Wang, R. Tan, X. Duan, T. Z. Tian, C. H Zhang, W.W. Xie, 2021 Roadmap: electrocatalysts for green catalytic processes, Journal of Physics: Material 4 (2021) 022004.

[50] X. Li, F. C Walsh, D. Pletcher, Nickel based electrocatalysts for oxygen evolution in high current density, alkaline water electrolysers. Physical Chemistry Chemical Physics 13 (2011) 1162-1167.

[51] V. Vij, Nickel-based electrocatalysts for energy-related applications: oxygen reduction, oxygen evolution, and hydrogen evolution reactions. Acs Catalysis 7 (2017) 7196-7225.

[52] M Kaur, P Chand, H. Anand Effect of different synthesis methods on morphology and electrochemical behavior of spinel $NiCo_2O_4$ nanostructures as electrode material for energy storage application, Inorganic Chemistry Communications 134 (2021) 108996.

[53] A. G. Solangi, T. Pirzada, A. A Shah, I. A Halepoto, A. S. Chang, Z. A Solangi, M. Y. Solangi, U Aftab, M. Tonezzer, A. Tahira, A. Nafady. Phytochemicals of mustard (Brassica Campestris) leaves tuned the nickel-cobalt bimetallic oxide properties for enzyme-free sensing of glucose, Journal of the Chinese Chemical Society. 69 (2022) 1608-18.

[54] A. Sivalingam, A Kandhasamy, A. Senthil Kumar, E. Perumal Venkatesan, L. Subramani, K Ramalingam, J. P Thadhani, H. Venu, A Citrullus colocynthis-an experimental investigation with enzymatic lipase based methyl esterified biodiesel. Heat and Mass Transfer 55 (2019) 3613-3631.

[55] S. Kiran, M. A. Rafique, S. Iqbal, S. Nosheen, S. Naz, A. Rasheed, Synthesis of nickel nanoparticles using Citrullus colocynthis stem extract for remediation of Reactive Yellow 160 dye. Environmental Science and Pollution Research 27 (2020) 32998-33007.

[56] I. A. Nehdi, H. M. Sbihi, L. E. Blidi, U. Rashid, C. P. Tan, S. I. Al-Resayes, Biodiesel production from Citrillus colocynthis oil using enzymatic based catalytic reaction and characterization studies. Protein and peptide letters 25 (2018) 164-170.

[57] A. M. Weli, S. Al-Salmi, H. Al Hoqani, Hossain MA.Biological and phytochemical studies of different leaves extracts of Pteropyrum scoparium. Beni-Suef University journal of basic and applied sciences 7 (2018) 481-486.

[58] M. B. Khan, H. Khan, M. U. Shah, S. Khan, Purification and biochemical properties of SDS-stable low molecular weight alkaline serine protease from Citrullus colocynthis.Natural product research 30 (2016) 935-940.

[59] B. Hameed, Q. Ali, M. M. Hafeez, A. Malik, Antibacterial and antifungal activity of fruit, seed and root extracts of Citrullus colocynthis plant. Biological and Clinical Sciences Research Journal 1 (2020) 42.

[60] S. Basharat, R. Rehman, T. Mahmud, S. Basharat, L. Mitu, Tartaric acid-modified Holarrhena antidysenterica and Citrullus colocynthis biowaste for efficient eradication of crystal violet dye from water. Journal of Chemistry 2020 (2020) 1-18.

[61] K. Tawfika, M. Al-Barazib, M. Bashirb, W. Al-Marzouq, R AlSoufib, H. Kharsab, A comparative study of antioxidant activities of ziziphus and colocynth from Saudi Arabia deserts and proposed pharmaceutical products, IRJPAS 5 (2015) 8-13.

[62] JA Kumar, T Krithiga, S Manigandan, S Sathish, AA Renita, P Prakash, BN Prasad, TP Kumar, M Rajasimman, A Hosseini-Bandegharaei, D Prabu. A focus to green synthesis of metal/metal based oxide nanoparticles: Various mechanisms and applications towards ecological approach. Journal of Cleaner Production. 324 (2021) 129-198.

[63] TL Chen TL, H Kim, SY Pan, PC Tseng, YP Lin, PC Chiang. Implementation of green chemistry principles in circular economy system towards sustainable development goals: Challenges and perspectives. Science of the Total Environment. 716 (2020) 136998.

819 [64] E Jokar, A.I. Zad, S. Shahrokhian, Synthesis and characterization of $NiCo_2O_4$ nanorods
820 for preparation of supercapacitor electrodes, J Solid State Electrochem 19 (2015) 269–
821 274.
822 [65] Y. Liu, Y. Zheng, Q. Xu, Y. Shi, Z. Tian, G. Zhang, J. Chen, Z. Wang, W.
823 Zheng, Controllable synthesis of $NiSe/MoSe_2/MoO_2$ 3D hierarchical hollow
824 microspheres with enhanced performance for asymmetric supercapacitors, Chem. Eng. J.
825 387 (2020) 124121.
826 [66] C. Young, R. R. Salunkhe, S. M. Alshehri, T. Ahamad, Z. Huang, J. Henzie, Y.
827 Yamauchi, High Energy Density Supercapacitors Composed of Nickel Cobalt Oxide
828 Nanosheets on Nanoporous Carbon Nanoarchitectures, J. Mater. Chem. A. 43 (2017)
829 11834-11839.
830 [67] F. Pellati, V. Brighenti, J. Sperlea, L. Marchetti, V. Bertelli, V. Benvenuti, New methods
831 for the comprehensive analysis of bioactive compounds in Cannabis sativa L.(hemp)
832 Molecules 23 (2018) 2639.
833 [68] A.A. Mariod, R.L. Jarret, Antioxidant, antimicrobial, and antidiabetic activities of
834 Citrullus colocynthis seed oil. InMultiple Biological Activities of Unconventional Seed
835 Oils, Academic Press 1 (2022) 139-146.
836 [69] N. Kahrom, V. Farzam, M. Mesdaghi, Habitat, Phenology, Seed Studies of Citrullus
837 colocynthis in Lut Desert. Iran, (2022).
838 [70] Ayan Yao, Hao Yang, Jun-Qiang Wang, Wei Xu, Juntao Huo, Run-Wei Li, Huajun Qiu,
839 Mingwei Chen, Flexible supercapacitor electrodes fabricated by dealloying
840 nanocrystallized Al-Ni-Co-Y-Cu metallic glasses, Journal of Alloys and Compounds, 77
841 (2019)164-172

[71] R. Kumar , S. Saho , E. Joanni , R. K. Singh , W. K. Tan , K. K. Kar and A. Matsuda , Recent progress in the synthesis of graphene and derived materials for next generation electrodes of high performance lithium ion batteries Progress Energy Combustion Sciences, 75(2019) 100786

[72] K. Harish, R. Renu, and S. R. Kumar, "Synthesis of nickel hydroxide nanoparticles by reverse micelle method and its antimicrobial activity," *Research Journal of Chemical Sciences*, 9(2011) 42–48

[73] Q. Song, Z. Tang, H. Guo, and S. L. I. Chan, Structural characteristics of nickel hydroxide synthesized by a chemical precipitation route under different pH values,*Journal of Power Sources*, 112 (2002)428–434,

[74] Z. Yang, C. Zhao, Y. Qu, H. Zhou, F. Zhou, J. Wang, Y. Wu, Y. Li, Trifunctional self-supporting cobalt-embedded carbon nanotube films for ORR, OER, and HER triggered by solid diffusion from bulk metal, Advanced Materials. 31 (2019) 1808043

[75] Z. H. bupoto, A. Tahira, A. A. Shah, U. Aftab, M. Y Solangi, J. A. Leghari, A. H. Samoon, A. L. Bhatti, M. A Bhatti, R. Mazzaro, V Morandi, $NiCo_2O_4$ nanostructures loaded onto pencil graphite rod: An advanced composite material for oxygen evolution reaction. International Journal of Hydrogen Energy 47 (2020) 6650-6665.

[76] P Zhou, J He, Y Zou, Y Wang, C Xie, R Chen, S Zang, S Wang. Single-crystalline layered double hydroxides with rich defects and hierarchical structure by mild reduction for enhancing the oxygen evolution reaction. Science China Chemistry. 62 (2019) 1365-70.

[77] Y.T. Lu, Y.J. Chien, C.F Liu, T. H. You, C. C. Hu, Active site-engineered bifunctional electrocatalysts of ternary spinel oxides, $M_{0.1}Ni_{0.9}Co_2O_4$ (M: Mn, Fe, Cu, Zn) for the

air electrode of rechargeable zinc–air batteries. Journal of Materials Chemistry A 5 (2017) 21016-21026.

[78] H.J. Lee, D.H. Park, W.J. Lee, S.B. Han, M.H. Kim, J.H. Byeon, K.W. Park, Mesoporous Spinel Ir-doped $NiCo_2O_4$ Nanostructure as an Efficient Catalyst for Oxygen Evolution Reaction, Applied Catalysis A: General 626 (2021) 118377.

[79] S.K. Li, A.Y. Chen, Y.Q. Chai, R. Yuan, Y. Zhuo, Electrochemiluminescence aptasensor based on cascading amplification of nicking endonuclease-assisted target recycling and rolling circle amplifications for mucin 1 detection, Electrochimica Acta. 212 (2016) 767-774.

[80] A.J. Laghari, U. Aftab, A. Tahira, A.A. Shah, A. Gradone, M.Y. Solangi, A.H. Samo, M.I. Abro, M. Wasim Akhtar, R. Mazzaro, V. Morandi, MgO as promoter for electrocatalytic activities of Co_3O_4–MgO composite via abundant oxygen vacancies and Co^{2+} ions towards oxygen evolution reaction, International Journal of Hydrogen Energy 48 (2023) 12672-82.

[81] X. Long, J. Li, S. Xiao, K. Yan, Z. Wang, H. Chen, S. Yang, A strongly coupled graphene and FeNi double hydroxide hybrid as an excellent electrocatalyst for the oxygen evolution reaction. Angewandte Chemie International Edition 53 (2014) 7584-7588.

[82] Y. Huang, L. Jiang, X. Liu, T. Tan, H. Liu, J. Wang, Precisely engineering the electronic structure of active sites boosts the activity of iron-nickel selenide on nickel foam for highly efficient and stable overall water splitting, Appl. Catal. B Environ. 299 (2021) 12067-80.

[83] H.F. Feng, S. Gao, J. Shi, L. Zhang, Z. Peng, S. Cao, Construction of 3D hierarchical porous $NiCo_2O_4$/graphene hydrogel/Ni foam electrode for high-performance supercapacitor. Electrochim. Acta. 299 (2019) 116–124.

[84] L. Zhang, H. Li, K. Li, L. Li, J. Wei, L. Feng, Q. Fu, Morphology-controlled fabrication of Co_3O_4 nanostructures and their comparative catalytic activity for oxygen evolution reaction, Journal of Alloys and Compounds 680 (2016) 146-54.

[85] S. Jiang, K. Ithisuphalap, X. Zeng, G. Wu, H. Yang, 3D porous cellular $NiCoO_2$/graphene network as a durable bifunctional electrocatalyst for oxygen evolution and reduction reactions, Journal of Power Sources 399 (2018) 66-75.

[86] C. Zhao, Q. Wang, Q. Zhang, H. Passerini, S. Qian, Two-Dimensional Titanium Carbide/RGO Composite for High-Performance Supercapacitors, ACS Appl. Mater. Interfaces 8 (2016) 15661–15667.

[87] A. Singh, A. Chandra, Enhancing Specific Energy and Power in Asymmetric Supercapacitors—A Synergetic Strategy based on the Use of Redox Additive Electrolytes. Sci. Rep. 6 (2016) 2579-03.

[88] Y Zhang, L Tao, C Xie, D Wang, Y Zou, R Chen, Y Wang, C Jia, S Wang. Defect engineering on electrode materials for rechargeable batteries. Advanced Materials. 32 (2020) 1905923.

[89] A.J. Mary, J.C. Sathish, C.R. Vinu, A.C. Bose, Electrochemical Performance of rGO/$NiCo_2O_4$@$ZnCo_2O_4$ Ternary Composite Material and the Fabrication of an all-Solid-State Supercapacitor Device. Energy Fuels 34 (2020) 10131–10141.

[90] E.M. Espinoza, E. Clark, J.A. Soliman, J. Derr, J.B. Morales, V.I. Vullev, Practical Aspects of Cyclic Voltammetry: How to Estimate Reduction Potentials When Irreversibility Prevails. J. Electrochem. Soc. 166 (2019) H3175–H3187.

[91] T. Kim, W. Choi, H.C. Shin, J.Y. Choi, J.M. Kim, M.S. Park, W.S. Yoon, Applications of voltammetry in lithium ion battery research, Journal of Electrochemical Science and Technology 11 (2020) 14-25.

[92] L.L. Zhang, X. Zhao, M.D. Stoller, Y. Zhu, H. Ji, S. Murali, Y. Wu, S. Perales, B. Clevenger, R.S. Ruoff, Highly conductive and porous activated reduced graphene oxide films for high-power supercapacitors, Nano letters 12 (2012) 1806-12.

[93] L. Zhang, G. Shi, Preparation of highly conductive graphene hydrogels for fabricating supercapacitors with high rate capability, The Journal of Physical Chemistry C. 115 (2011) 17206-12.

[94] C. Wan, W. Tian, J. Zhou, Y. Qing, Q. Huang, X. Li, S. Wei, L. Zhang, X. Liu, Y. Wu, Green anisotropic carbon-stabilized polylaminate copper oxide as a novel cathode for high-performance hybrid supercapacitors. Materials & Design 198 (2021) 109309.

Supporting Information

Electronic and structural disorder of $NiCo_2O_4$ Nanostructures using phytochemicals from desert gourd offered efficient asymmetric supercapacitor and oxygen evolution reaction

Shusheel Kumar[a], Aneela Tahira[c], Adeel Liaquat Bhattia, Umair Aftab[e], Ayman Nafady[k], Sooraj Kumar[d], Mélanie Emo[f], Brigitte Vigolo[f], Antonia Infantes-Molin[g], Elmuez Dewai[j], Alberto Vomiero[h,i*], Zafar Hussain Ibupoto[*b]

[a]Institute of Physics, University of Sindh Jamshoro, 76080, Sindh Pakistan

[b]Institute of Chemistry, University of Sindh Jamshoro, 76080, Sindh Pakistan

[c]Institute of Chemistry, Shah Abdul Latif University Khairpur Mirs, Sindh, Pakistan

[d]Department of Chemical Engineering, Mehran University of Engineering and Technology, 7680 Jamshoro, Sindh Pakistan

[e]Department of Metallurgy and Materials, Mehran University of Engineering and Technology, 7680 Jamshoro, Sindh Pakistan

[f]Université de Lorraine, CNRS, IJL, F-54000 Nancy, France

[g]Department of Inorgnic Chemistry, Crystallography and Mineralogy. (Unidad Asociada al ICP-CSIC), Faculty of Sciences, University of Malaga, Campus de Teatinos, 29071, Malaga, Spain

[h]Department of Engineering Sciences and Mathematics, Division of Material Science, Luleå University of Technology, Luleå, Sweden

[i]Department of Molecular Sciences and Nanosystems, Ca' Foscari University of Venice, Venezia Mestre, Italy

[j]Nonlinear Dynamics Research Centre (NDRC), Ajman University, P.O. Box 346, United Arab Emirates.

[j]Chemistry Department, College of Science, King Saud University, Riyadh, 11451, Saudi Arabia

*__Corresponding authors__: Alberto Vomiero and Zafar Hussain Ibupoto

Email: zaffar.ibhupoto@usindh.edu.pk

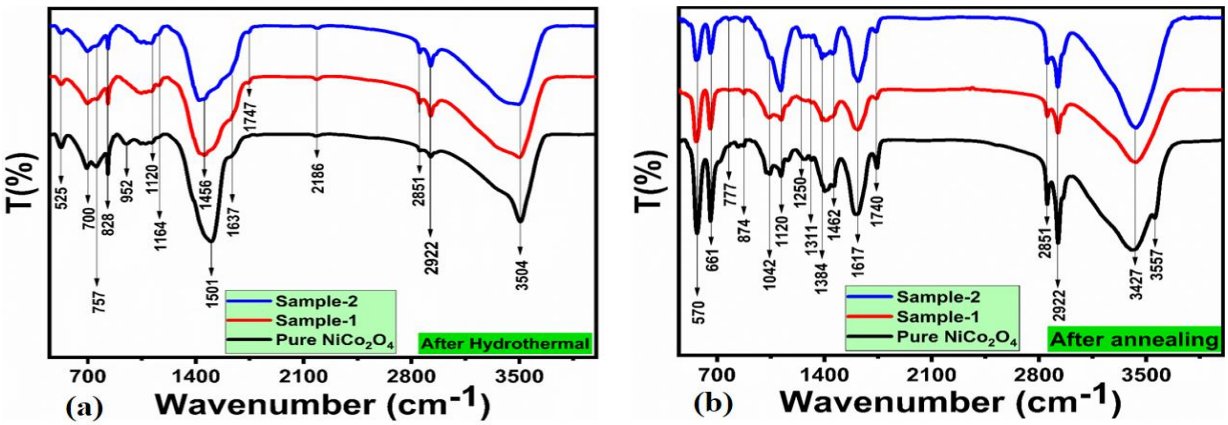

962

963 **S1:** FTIR spectra after hydrothermal and annealing process for pure $NiCo_2O_4$ and desert gourd
964 juice assisted synthesized sample-1 and sample -2

965

966

967

968

969

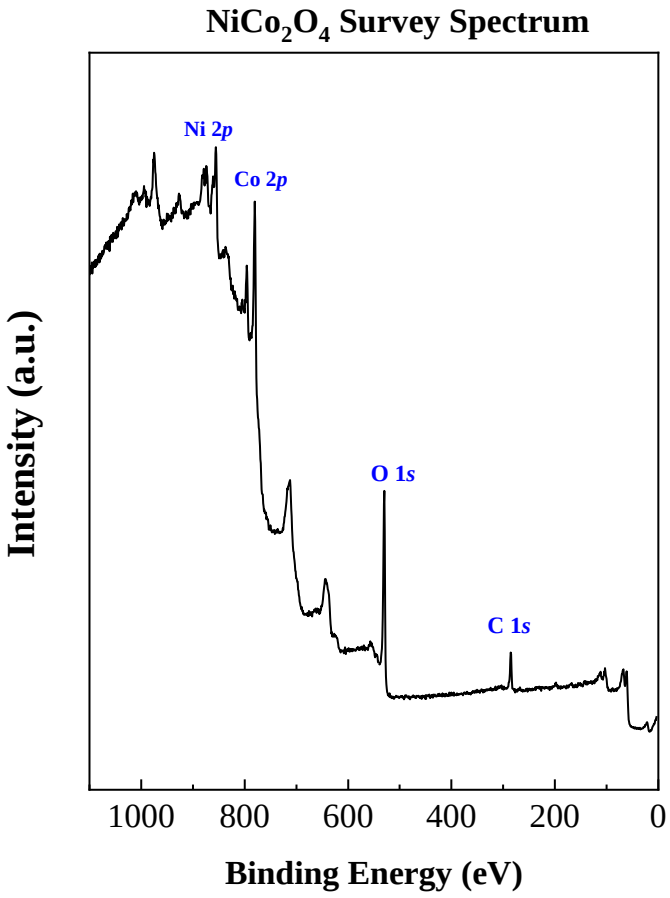

970

971

972

973 **S2:** Wide scan survey of pure $NiCo_2O_4$

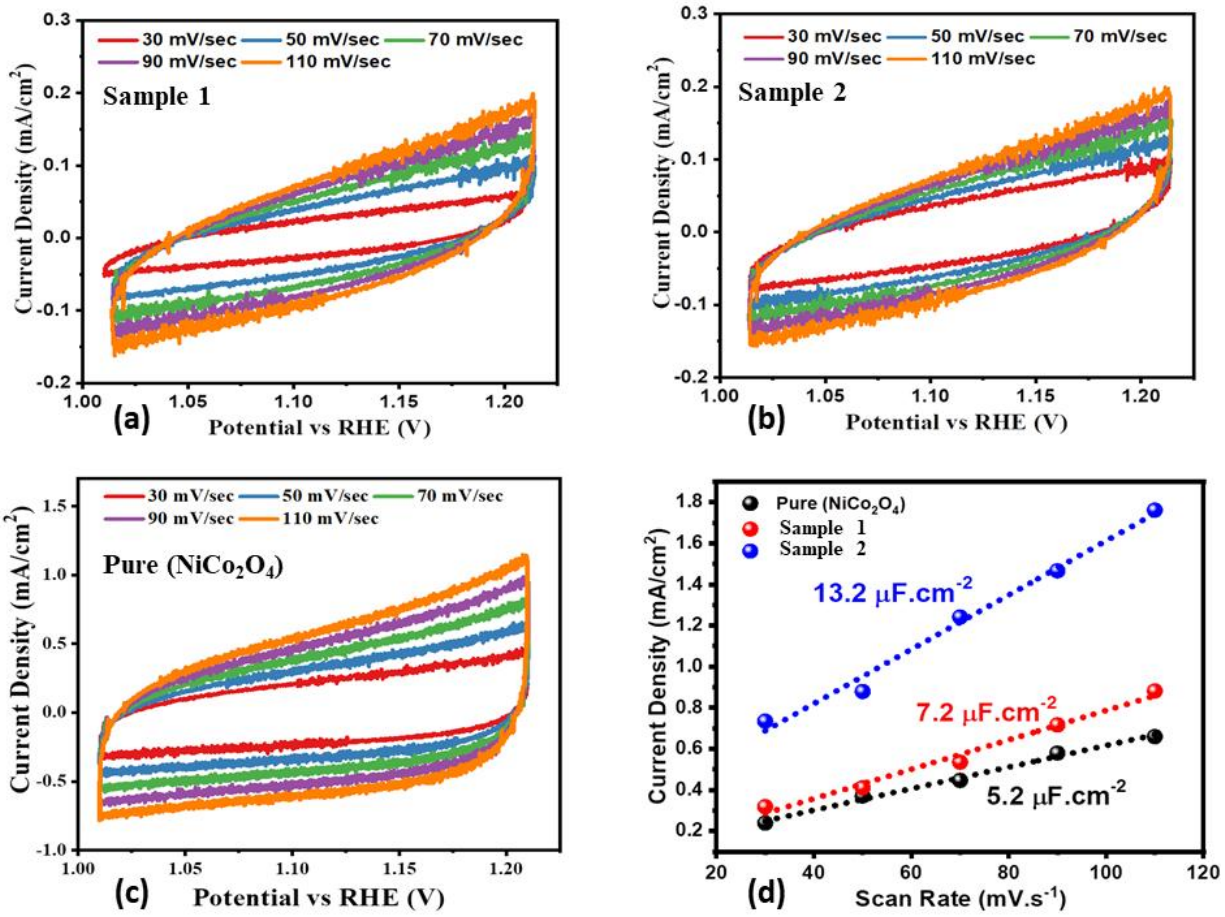

974

975 **S3:** Various CV curves measured in 1.0M KOH at differrnt scan rates (a) $NiCo_2O_4$
976 nanostructure (sample 1) (b) $NiCo_2O_4$ nanostructure (sample 2) and (c) pure $NiCo_2O_4$
977 nanostructure (d) estimated ECSA from non-Faradic region of recorded CV curevs for pure
978 $NiCo_2O_4$ nanostructure, $NiCo_2O_4$ (sample 1), $NiCo_2O_4$ nanostructure (sample 2).

979

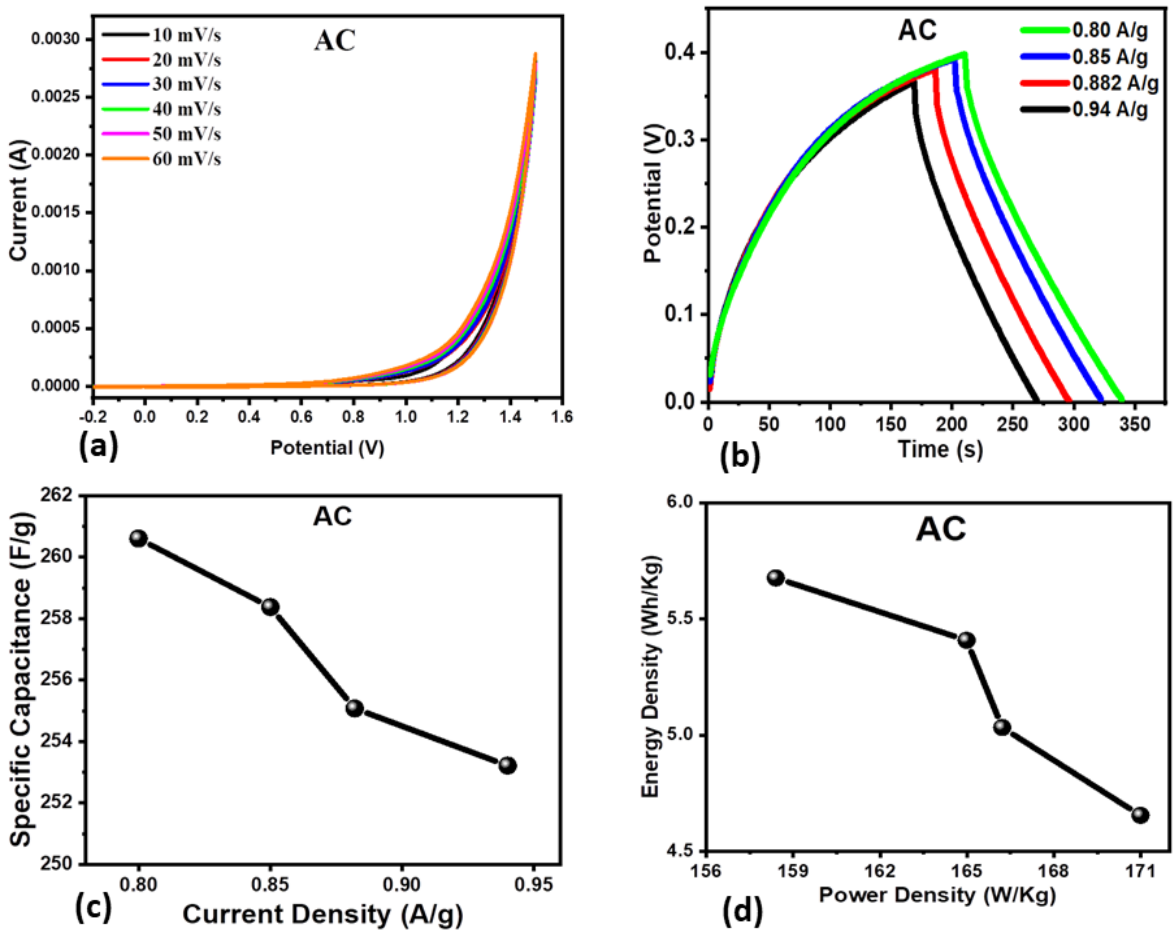

S4: Recorded CV curves of activated carbon (AC) in 3.0M KOH at different scan rates , (b) GCD curves of AC in 3.0M KOH at various current density (c) specific capacitance (Cs) from GCD curves of AC, (d) Energy density of AC in 3.0M KOH obtained from various GCD curves

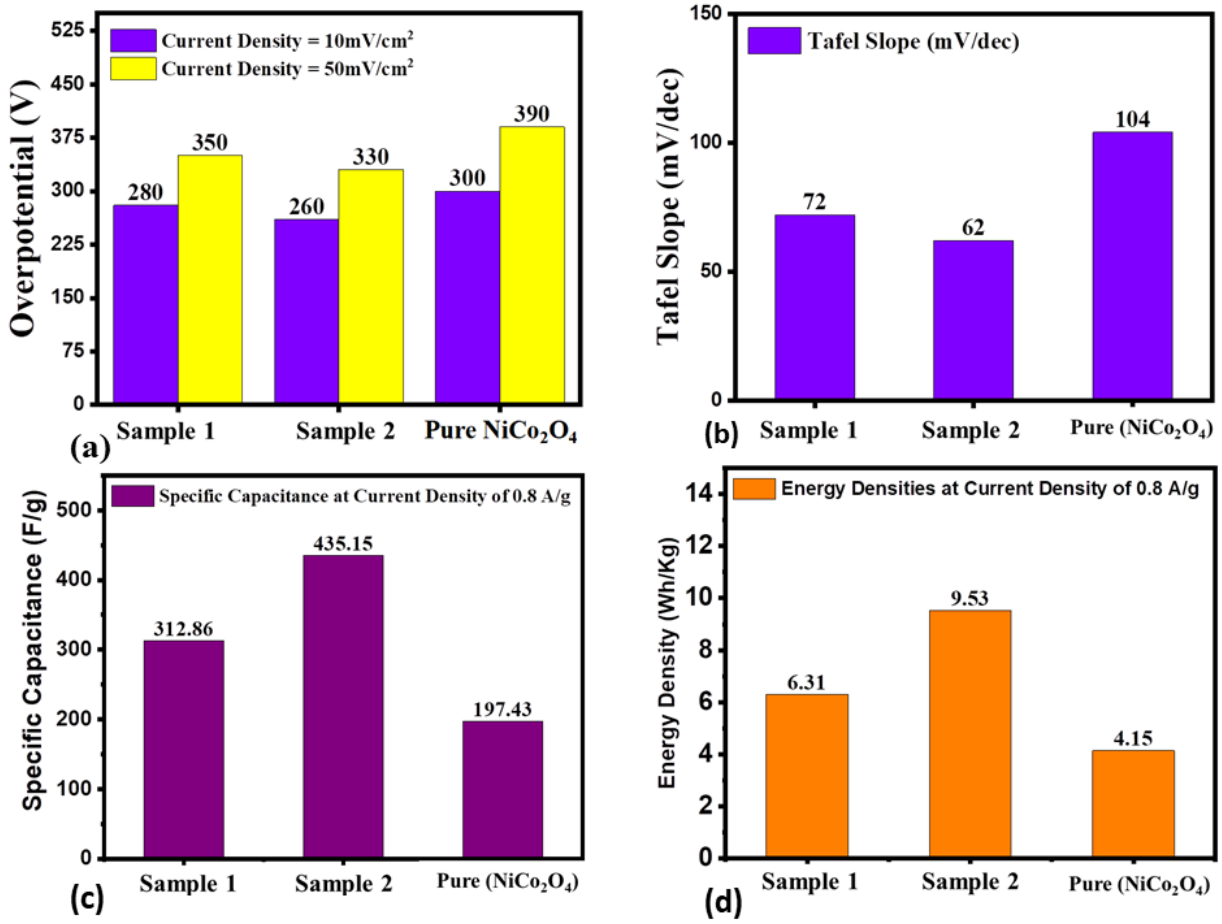

S5: Bar graph view Bar graph view (a) overpotential at 10 and 50 $mAcm^{-2}$ for pure $NiCo_2O_4$ nanostructure, $NiCo_2O_4$ (sample 1), $NiCo_2O_4$ (sample 2) in 1.0M KOH (b) Tafel slope for pure $NiCo_2O_4$ nanostructure, $NiCo_2O_4$ (sample 1), $NiCo_2O_4$ (sample 2) in 1.0M KOH, (c) specific capacitance (Cs) for pure $NiCo_2O_4$ nanostructure, $NiCo_2O_4$ (sample 1), $NiCo_2O_4$ (sample 2) in 3.0M KOH (d) Energy density of supercapacitor for pure $NiCo_2O_4$ nanostructure, $NiCo_2O_4$ (sample 1), $NiCo_2O_4$ (sample 2) in 3.0M KOH.

997 **Table (S1):** The calculated supercapacitor indicators for_$NiCo_2O_4$ nanostructures sample 1,

998 sample 2 and pure $NiCo_2O_4$.

Samples	Current Density (A/g)	Specific capacitance (F/g)	Energy density (Wh/kg)	Power Density (W/kg)	Columbic Efficiency %	Capacitance Retention %
Sample 1	0.8	313	6	152	66%	110-80%
	0.85	277	6	163		
	0.882	179	4	172		
	0.94	106	2	183		
Sample 2	0.8	435	10	159	74%	103-93%
	0.85	298	7	168		
	0.882	197	4	174		
	0.94	176	4	188		
Pure ($NiCo_2O_4$)	0.8	197	4	156	52%	88-60%
	0.85	128	3	167		
	0.882	110	2	174		
	0.94	94	2	183		

999

1000

1001

1002

1003

1004

1005

1006

1007

Table (S2): Calculated values of specific capacitance, energy density and power density of activated carbon using three electrode cells set up.

Samples	Current Density (A/g)	Specific capacitance (F/g)	Energy density (Wh/kg)	Power Density (W/kg)
Activated Carbon	0.8	261	6	158
	0.85	258	5	165
	0.882	255	5	166
	0.94	253	5	171

Table (S3): Supercapacitor performance evaluation of $NiCo_2O_4$ nanostructure prepared with desert gourd fruit juice (sample 2, T-2) with reported supercapacitors based on $NiCo_2O_4$.

Material	Specific Capacitance (F/g)	Current Density (A/g)	Potential Window (V)	Energy Density (Wh/kg)	Power Density (W/kg)	References
NCO@MWCNT	374	2	-0.5 to 2.2	95	3964	[1]
MWCNTs	84	0.6	-0.5 to 2.2	21	6237	[1]
NCO//MWCNT	157	0.6	-0.5 to 2.2	40	2816	[1]
NCO@MWCNT// MWCNT	242	0.6	-0.5 to 2.2	61	2837	[1]
NiCoF	50	1	0 to 1	-	-	[2]
NiCuF	44	1	0 to 1	-	-	[2]
NC6	1294.25	10	0.4	-	-	[3]
NC10	687.20	10	0.4	-	-	[3]
$NiCo_2O_4$ (Desert Gourd)	435	0.8	0 to 0.4	9.53	159	This Work

Table (S4): The summary of OER activity performance of Desert Gourd juice assisted $NiCo_2O_4$ nanostructures with recently reported electrocatalysts in 1.0 M KOH.

Catalyst	Over potential (mV) @ 10 mA/cm^2	Electrolyte	References
$NiCo_2O_4$@Graphene Nano sheets	383	1.0 M KOH	[4]
NiOx/$NiCo_2O_4$/Co_3O_4	315	1.0 M KOH	[5]
$NiCo_2O_4$/CoO/graphite	323	1.0 M KOH	[6]
MOF derived-$NiCo_2O_4$/NiO	430	1.0 M KOH	[7]
P-doped $NiCo_2O_4$ on Ni-Foam	300	1.0 M KOH	[8]
Co_8FeS_8/CoS@CNT	278	1.0 M KOH	[9]
CoSx/MoS_2	347	1.0 M KOH	[10]
$NiCo_2O_4$/NiO	360	1.0 M KOH	[11]
CoxNi1-xS_2 (CNS)/rGO	290	1.0 M KOH	[12]
3D core–shell $NiCo_2O_4$@CoS/NF	290	1.0 M KOH	[13]
CoFe/Co_8FeS_8/CNT	290	1.0 M KOH	[14]
$NiCo_2O_4$/NiO hexagonal rods	285	1.0 M KOH	[15]
Ni_3S_2/MoS_2 (NiMoS)	260	1.0 M KOH	[16]
Ni3N-NiMoN	277	1.0 M KOH	[17]
Co_3O_4@CMC	290	1.0 M KOH	[18]
Desert Gourd assisted $NiCo_2O_4$ material	**260**	**1.0 M KOH**	**Present Work**

Reference

[1] M. Pathak, J.R. Jose, B. Chakraborty, C.S. Rout, High performance supercapacitor electrodes based on spinel NiCo2O4@ MWCNT composite with insights from density functional theory simulations, The Journal of Chemical Physics. 152 (2020) 064706.

[2] B. Bhujun, M.T. Tan, A.S. Shanmugam, Study of mixed ternary transition metal ferrites as potential electrodes for supercapacitor applications, Results in Physics 7 (2017) 345-53.

[3] M. Kaur, P. Chand, H. Anand, Binder free electrodeposition fabrication of NiCo2O4 electrode with improved electrochemical behavior for supercapacitor application, Journal of Energy Storage 52 (2022) 104941.

[4] Z. Li, B. Li, J. Chen, Q. Pang, P. Shen, Spinel NiCo2O4 3-D nanoflowers supported on graphene nanosheets as efficient electrocatalyst for oxygen evolution reaction, International Journal of Hydrogen Energy 44 (2019) 16120-31.

[5] J. Chen, Y. Ling, Z. Lu, X. Huai, F. Qin, Z. Zhang, Sandwich-like NiOx/NiCo2O4/Co3O4 nanoflakes enable efficient oxygen evolution electrocatalysis, Electrochimica Acta 322 (2019) 134753.

[6] N. Srinivasa, L. Shreenivasa, P.S. Adarakatti, J.P. Hughes, S.J. Rowley-Neale, C.E. Banks, S. Ashoka, In situ addition of graphitic carbon into a NiCo 2 O 4/CoO composite: enhanced catalysis toward the oxygen evolution reaction, RSC advances 9 (2019) 24995-5002.

[7] Y. Wang, Z. Zhang, X. Liu, F. Ding, P. Zou, X. Wang, Q. Zhao, H. Rao, MOF-derived NiO/NiCo2O4 and NiO/NiCo2O4-rGO as highly efficient and stable electrocatalysts for oxygen evolution reaction. ACS Sustainable Chemistry & Engineering 6 (2018) 12511-21.

[8] W. Chu, Z. Shi, Y. Hou, D. Ma, X. Bai, Y. Gao, N. Yang, Trifunctional of phosphorus-doped NiCo2O4 nanowire materials for asymmetric supercapacitor, oxygen evolution reaction, and hydrogen evolution reaction. ACS applied materials & interfaces 12 (2019) 2763-72.

[9] B. Wang, Y. Chen, X. Wang, X. Zhang, Y. Hu, B. Yu, D. Yang, W. Zhang, A microwave-assisted bubble bursting strategy to grow Co8FeS8/CoS heterostructure on rearranged carbon nanotubes as efficient electrocatalyst for oxygen evolution reaction. Journal of Power Sources 449 (2020) 227561.

[10] L. Yang, L. Zhang, G. Xu, X. Ma, W. Wang, H. Song, D. Jia. Metal–Organic-Framework-Derived Hollow CoS x@ MoS2 Microcubes as Superior Bifunctional Electrocatalysts for Hydrogen Evolution and Oxygen Evolution Reactions, ACS Sustainable Chemistry & Engineering 6 (2018) 12961-8.

[11] C. Mahala, M. Basu. Nanosheets of NiCo2O4/NiO as efficient and stable electrocatalyst for oxygen evolution reaction. ACS omega 2 (2017) 7559-67.

[12] Y.R. Hong, S. Mhin, K.M. Kim, W.S. Han, H. Choi, G. Ali, K.Y. Chung, H.J. Lee, S.I. Moon, S. Dutta, S. Sun, Electrochemically activated cobalt nickel sulfide for an efficient oxygen evolution reaction: partial amorphization and phase control, Journal of Materials Chemistry A. 7 (2019) 3592-602.

[13] S. Adhikari, Y. Kwon, D.H. Kim, Three-dimensional core–shell structured NiCo2O4@ CoS/Ni-Foam electrocatalyst for oxygen evolution reaction and electrocatalytic oxidation of urea, Chemical Engineering Journal 402 (2020) 126192.

[14] B. Wang, Y. Hu, B. Yu, X. Zhang, D. Yang, Y. Chen, Heterogeneous CoFe–Co8FeS8 nanoparticles embedded in CNT networks as highly efficient and stable electrocatalysts for oxygen evolution reaction. Journal of Power Sources 433 (2019) 126688.

[15] Y. Yuan, L. Sun, Y. Li, W. Zhan, X. Wang, X. Han, Synergistic modulation of active sites and charge transport: N/S Co-doped C encapsulated NiCo2O4/NiO hollow microrods for boosting oxygen evolution catalysis. Inorganic Chemistry 59 (2020) 4080-9.

[16] C. Wang, X. Shao, J. Pan, J. Hu, X. Xu, Redox bifunctional activities with optical gain of Ni3S2 nanosheets edged with MoS2 for overall water splitting. Applied Catalysis B: Environmental 268 (2020) 118435.

[17] A. Wu, Y. Xie, H. Ma, C. Tian, Y. Gu, H. Yan, X. Zhang, G. Yang, H. Fu, Integrating the active OER and HER components as the heterostructures for the efficient overall water splitting, Nano Energy 44 (2018) 353-63.

[18] A.L. Bhatti, A. Tahira, A. Gradone, R. Mazzaro, V. Morandi, M.I. Abro, A. Nafady, K. Qi, A. Infantes-Molina, A. Vomiero, Z.H. Ibupoto, Nanostructured Co3O4 electrocatalyst for OER: the role of organic polyelectrolytes as soft templates, Electrochimica Acta. 398 (2021) 139338.